NTNU – Trondheim
Norwegian University of
Science and Technology

Carbon Based Coatings for Metallic Bipolar Plates in PEM Fuel Cells

Håvard Husby

Chemical Engineering and Biotechnology
Submission date: June 2013
Supervisor: Frode Seland, IMTE

Norwegian University of Science and Technology
Department of Materials Science and Engineering

Preface

This report describes the work carried out during the master thesis (TMT4900) in the spring of 2013. The report is the final submission to complete the master's degree in Industial Chemistry and Biotechnolgy at the Norwegian University of Science and Technology (NTNU) in Trondheim. Associate professor Frode Seland has been my supervisor during this work. I would like to express my thanks to him for his guidance, feedback and supervision.

The project has been collaborate effort between NTNU and SINTEF, and is a part of the European project STAMPEM. This is a project where SINTEF and partners work on developing coatings for bipolar plates for PEM fuel cells. The partners include research institutions and the industry. SINTEF employees Dr. Anders Ødegård and Dr. Ole Edvard Kongstein have been my co-supervisors. I would like to thank them for all the help and guidance I have received.

I would like to express my gratitude to Ph.D candidate Sigrid Lædre and Angelica Orsi, visiting master student from St. Andrews, for valuable discussions and guidance, both work related and otherwise. You both helped make the long lab hours go by faster.

I would also like to thank the girls that make my coffee breaks unpredictable and interesting, as well as frequent at times. You know who you are.

Finally I would like to thank the girl I can come home to every evening. You are my most valuable asset.

Declaration

I, Håvard Husby, declare that the work described in this report has been done in accordance with the regulations at NTNU.

Trondheim, June 2013

Håvard Husby

Abstract

Global warming and the climate changes are issues that concern everyone. The transition to other energy carriers than fossil fuels is a key barrier if we are to reduce our dependence on oil. Hydrogen is forecasted as the energy carrier of the future, and one of the most efficient ways to convert hydrogen to electrical, useful energy is to feed it to the anode side of a polymer electrolyte (PEM) fuel cell. Oxygen (usually in the form of air) is supplied to the cathode side and the only products are water, electricity and some heat.

A key component in PEM fuel cells are the bipolar plates that facilitate gas flow, electron transfer, heat and water removal. The bipolar plates contribute greatly to both weight and cost of PEM fuel cells, and there is continuous development in making cheap, durable, light and efficient bipolar plates.

In this work we attempted to coat stainless steel (316L) plates with a coating consisting of graphite and carbon black mixed with epoxy. The goal was to get a coating that conducts electrons while still protecting against corrosion. The coatings were sought further improved by adding Teflon particles. This was done to get the coating more hydrophobic, and thus a better corrosion protection of the underlying stainless steel substrate. Plates were glass blasted prior to coating to improve adhesion.

Coatings were thinned with xylene and sprayed onto the plates with an air brush. The plates were then pressed in a "Carver" hot-press to achieve minimum porosity. The coated plates were examined in a contact resistance apparatus, subjected to linear sweep voltammetry and chronoampereometry, the contact angles were measured, the surface roughness measured and SEM images are taken.

Plates pressed at 2670 N cm^{-2} for 30 minutes with 4.8 vol% Zonyl in the

coating performed best prior to electrochemical measurements both for the glass blasted plates and for the as-delivered plates. The contact resistances measured at 147 N cm^{-2} compaction pressure was 11.3 and 10.6 mΩ cm^2 respectively. This is close to the goals set by DOE to reached by 2020 (10 mΩ cm^2 at 138 N cm^{-2}). The contact resistances for all coatings tested increased very much after the electrochemical testing, and all were far above the goals set by DOE.

A correlation was found between the coating thickness and the current densities measured during the potentiostatic measurements. The current densities increased with increasing coating thickness. Possible mechanisms and reasons for this are discussed, and a combination of carbon corrosion and crevice corrosion is suggested as explanation.

A possible method for anchoring the coating to the substrate while protecting the contact points from degradation during electrochemical measurements was suggested. By pressing the coating into carefully controlled voids, connections between the graphite in the coating and the metal substrate might be retained, even if the connection between main substrate surface and the coating is broken. This effect can explain the differences seen between the plates coated in the project work, and the metal sheets coated in this work.

Sammendrag

Global oppvarming og klimaendringer er temaer som angår alle. Overgangen til andre energibærere enn fossile brensler er en viktig hindring som må overkommes om vi skal minske vår avhengighet av olje. Hydrogen er foreslått som fremtidens energibærer, og en av de mest effektive måtene å omdanne hydrogen til brukbar, elektrisk energi er i en PEM (polymer electrolytt membran) brenselcelle. Brenselcellen forbruker hydrogengass og oksygengass (vanligvis fra luft), og det eneste utslippet er vann.

En viktig komponent i PEM brenselceller er de bipolare platene som sørger for gasstransport, elektronoverføring, varme- og vannfjerning. De bipolare platene bidrar i stor grad til både vekten og kostnadene til PEM brenselceller, og det er pågående forskning for å utvikle billige, holdbare, lette og effektive bipolare plater.

I dette arbeidet forsøkte vi å dekke rustfrie (316L) stålplater med en maling bestående av grafitt og carbon black blandet med en epoxypolymer. Målet var å få en maling som leder elektroner samtidig som den beskytter mot korrosjon. Malingen ble så forsøkt forbedret ved å tilsette Teflon partikler. Dette ble gjort for å øke hydrofobisiteten til malingen, og på den måten gjøre den mer korrosjonsbestandig. Plater ble også glassblåst før de ble malt for å få bedre feste til malingen.

Malingene ble fortynnet med xylen og sprayet på platene med en luftpensel. Platene ble så presset i en "Carver" varmepresse for å oppnå så liten porositet som mulig. De malte platene ble undersøkt i kontaktmotstandsoppsett, testet elektrokjemisk ved linær sveip voltametri og chronoamperoomeri, kontaktvinkler ble målt, overflateruheten undersøkt og SEM bilder ble tatt av overflatene.

Plater som ble presset ved 2670 N cm^{-2} i 30 minutter med 4.8 vol% Zonyl i malingen gjorde det best før de elektrokjemiske målingene, både for de

glassblåste og de ubehandlede platene. Kontaktmotstanden målt ved 147 N cm^{-2} kompresjonstrykk var 11.3 og 10.6 mΩ cm^2 for henholdsvis glassblåste og ubehandlede plater. Dette er ikke så langt ifra målene som er satt av det amerikanske energidepartementet (DOE) å bli nådd før 2020. Disse målene er på 10 mΩ cm^2 ved 138 N cm^{-2} kompresjonstrykk. Kontaktmotstanden for alle malingene økte veldig mye etter de elektrokjemiske målingene, og alle var langt over målet som er satt av DOE.

Det ble funnet en sammenheng mellom malingstykkelse og strømtetthetene målt under de potensiostatiske målingene. Strømtettheten ser ut til å øke ved økende malingstykkelse. Mulige mekanismer og grunner til dette blir diskutert, og en kombinasjon av karbonkorrosjon og spaltekorrosjon blir foreslått som årsak.

En mulig metode for å forankre den ledende malingen til substratet samtidig som kontaktpunktene mellom substratet og grafitten i malingen beskyttes fra degradering under elektrokjemiske målinger er foreslått. Ved å presse malingen inn i tynne hulrom kan koblingene mellom grafitten og substratet bestå, selv om koblingene mellom grafitt og overflaten på substratet blir brutt. Denne effekten kan forklare forskjellene i kontaktmotstandsresultater fra prosjektarbeidet og fra dette arbeidet.

Abbreviations

Abbreviation	Description
AFC	Alkaline Fuel Cell
CB	Carbon Black
CNC	Carbon Nano Cage
CNT	Carbon Nano Tube
DMFC	Direct Methanol Fuel Cell
GDL	Gas Diffusion Layer
ICR	Interfacial Contact Resistance
MCFC	Molten Carbonate Fuel Cell
SHE	Standard Hydrogen Electrode (0V, a_{H^+}=a_{H_2}=1)
SOFC	Solid Oxide Fuel Cell
PAFC	Phosphorous Acid Fuel Cell
PEM	Proton Exchange Membrane (Polymer Electrolyte Membrane)
PEMFC	Proton Exchange Membrane Fuel Cell
PTFE	PolyTetraFluoroEthylene
PVD	Physical Vapor Deposition

Nomenclature

Symbol	**Description**	**Unit**
A_a	Apparent contact area	m^2
D	Fractal dimentions of a surface profile	-
E	Potential	V
γ_i	Surface tension of i	Nm^{-1}
G	Topothesy of a surface profile	m
I	Current	A
j	Current density	Acm^{-2}
κ	Electrical conductivity	Sm^{-1}
K	Geometric constant	-
p	Compaction pressure	Ncm^{-2}
R_C	Interfacial contact resistance	Ωcm^2
R_{Rough}	Ratio actual/projected area	-
S	Scan length	m
Θ	Contact angle	-

Contents

Chapter 1

Introduction

The anthropogenic contribution to global warming has been evident for some time. To reduce the impact we have on the climate, it is important to minimize the use of fossil fuels. A potential energy carrier that can replace fossil fuels is hydrogen. Hydrogen can be made from water splitting, and can be made sustainable with the use of renewable energy. This can afterwards be converted to electrical energy in a fuel cell, without any emissions other than water.

Proton exchange membrane (PEM) fuel cells are compact fuel cells that typically operate at temperatures below 100 $^{\circ}C$. A proton conducting polymer membrane is packed between two gas diffusion layers (GDL). The membrane assembly is then packed between two flow fields. These distribute hydrogen and oxygen, and remove the exhaust products (water, unreacted gases and air, if air is used for oxygen supply). PEM fuel cells are the chosen alternative for use in cars, due to their low volume, compressibility and low operating temperature [1].

Current fuel cell technology is too expensive and have too low "well to wheel" efficiencies to successfully compete with the traditional internal combustion engines [1]. One of the main costs and weight contributions to fuel cells are the bipolar plates.

In the literature there are many examples of coating stainless steel plates with carbon based materials. Reported work give examples of chemical vapour deposition [2], conducting polymer deposition by electrochemical methods [3]. Multifunctional silane with conductive carbon black [4], and yet other coated the bipolar plates with an epoxy/graphite paste by blade

coating [5]. There are also many other methods used.

In this work we aim to find a cost efficient way to get a low contact resistance between the metallic bipolar plates (BPP) and the gas diffusion layer (GDL), and keep it low after electrochemical measurements. This would increase the efficiency of the cell, and at the same time retain the mechanical strength of stainless steel.

The goal for this project is to make an epoxy/carbon/Zonyl composite and apply this to the surface of the BPPs. This is done by thinning the epoxy/carbon/Zonyl mix with xylene, and air brushing the mixture onto the BPPs. They are then placed in a hot press and pressed at elevated temperatures to remove porosity. After making the plates, they are characterized by the use of interfacial contact resistance (ICR) measurements, potentiostatic and potentiodynamic measurements, contact angle measurements, scanning light microscopy (SLM) and scanning electron microscopy (SEM).

The project has been collaborate effort between NTNU and SINTEF, and is a part of the European project STAMPEM. This is a project where SINTEF and partners work on developing coatings for bipolar plates for PEM fuel cells. The partners include research institutions and the industry.

The work is a continuation of the work done by Hans Husby [6] in his master thesis on carbon composite coatings for bipolar plates. The recipe for the paint that was developed is the one that is used as a basis in this project. The chosen environment for electrochemical testing was developed by Sigrid Lædre [7] in her master thesis on metal bipolar plates for PEM fuel cells.

Chapter 2

Background

PEM fuel cells are an option to internal combustion engines in vehicles, as well as for stationary systems. Their main benefit is that they are not bound by the Carnot efficiency [8], since they do not depend on heat transfer to convert the chemical energy into electrical energy. The fuel cells therefore have higher theoretical fuel efficiency than combustion engines at low temperatures ($<400\ ^{\circ}C$). The main drawback for the fuel cells is the cost of manufacture, and the durability of the cells [9].

Traditionally, the main cost of the (PEM) fuel cells has been the cost of platinum catalyst. This has in the later years shifted, as less catalyst is being used in modern fuel cells. For further cost reduction it is therefore important to focus on the other parts of the fuel cell.

The bipolar plates contribute to a large fraction of both the cost and volume of the fuel cell. The plates need to be electrically conducting, as well as corrosion resistant to be used inside a fuel cell. Stainless steel is the chosen material in most fuel cells today, because of its corrosion resistance and relatively good electrical conductivity. Tawfik et al. argue in their review that the reduction in conductivity comes mainly from the insulating chromium oxide at the surface of the stainless steel plates [10].

Another type of bipolar plates is ceramic carbon plates. These have a very good corrosion resistance, and electrical conductivity, but are more brittle than steel. They thus need to be made in thicker slabs.

This project aims to combine the good qualities from both options, by coating the steel bipolar plates with a conducting layer of carbon in epoxy

paint. The principle has been investigated before [2, 6, 11], but there is still much work to be done.

The corrosion properties of the coated bipolar plates is sought improved by adding Zonyl, which is small particles of hydrophobic PolyTetraFluorEthene (PTFE), to the coatings. The adhesion of the coating is attempted improved by glass blasting the plates prior to coating.

Chapter 3

Theory

3.1 Fuel Cells

In an ideal fuel cell, all the Gibbs energy is converted into electrical energy. Gibbs energy can be seen as a measure of the energy available to do external work, neglecting work done by changes in pressure or volume. The change in Gibbs energy for an reaction can be expressed as [3.1].

$$\Delta G = \Delta H - T\Delta S \tag{3.1}$$

ΔH is the latent energy available for transferring electrons (Enthalpy), T is the absolute temperature (in Kelvin) and ΔS is the change in entropy. The total change in entropy has to increase for a reaction (Thermodynamic 2. law), and since the entropy of the system decreases (1.5 gas molecules goes to 1 gas molecule, see equation 3.4), the entropy of the surroundings has to increase. This in practice gives an heat exchange with a magnitude $T\Delta S_{ext}$ even when the cell is run reversibly.

There will in real systems always be some degree of irreversibility (heat production), but the net goal is still the same; to efficiently convert chemical energy into electrical energy [8].

A fuel cell basically consist of a membrane selectively permeable for an ion, but insulating for electrons. The reactants are being supplied to both sides of a membrane. On one side the reactant gets reduced to the corresponding ion and electrons. On the other side of the membrane an oxidation occurs which consumes electrons. Depending on the membrane chosen, either the

reduced specie or the oxidized specie passes through the membrane and reacts with the opposite specie. The electrons are forced to pass through an outer circuit, where the electrical energy can be utilized. The reaction continues as long as fuels are being supplied.

The ideal fuel for fuel cells is pure hydrogen, being fed on the anode side and oxygen on the cathode side. Oxygen is abundant in air, so commonly a compressor or fan for air is used to supply the oxygen needed. The charge carrier in the electrolyte, closing the circuit, can vary for different fuel cells. The most common varieties of fuel cells are alkaline fuel cells (AFC), proton exchange membrane fuel cells (PEMFC), direct methanol fuel cell (DMFC), phosphoric acid fuel cell (PAFC), molten carbonate fuel cell (MCFC) and solid oxide fuel cells (SOFC). The fuel cells and their chemical reactions are summarized in Table 3.1.

Table 3.1: The most common types of fuel cells [12].

Cell Type	**Mobile Ion**	**Electrolyte**	**Operating Temp.** $[^{\circ}C]$
AFC	OH^-	Liquid Alkaline sol.	50-200
PEMFC	H^+	Solid Polymer	30-100
DMFC	H^+	Solid Polymer	20-90
PAFC	H^+	Liquid Phosph. Acid	~ 220
MCFC	CO_3^{2-}	Molten carbonate	~ 650
SOFC	O^{2-}	Solid Oxide	500-1000

3.1.1 PEM Fuel cells

The focus for this work will be PEM fuel cells. These cells are the most relevant for use in automotive transportation, as they are relatively compact, operate at low temperatures and have a solid electrolyte [12]. As the public become more aware of the anthropogenic contribution to the climate changes, the need for a future reduction in fossil fuel use is becoming clear. One of the possible energy carriers for the future is hydrogen. Most automotive manufacturing companies have ongoing research on hydrogen powered vehicles and participate in large international research programs with hydrogen storing companies and hydrogen producers. Hyundai announced in late February that their first mass produced hydrogen powered car had rolled out of their factory in South Korea [13]. Daimler is scheduled to follow during 2014, while practically all other producers are scheduled for 2015.

The first demonstration of the principles of a hydrogen fuel cell was given by Sir William Robert Grove in 1839 [8]. He used a simple setup like the one shown in Figure 3.1 , where he first electrolyzed water into hydrogen gas and oxygen gas, and then replaced the power source with an ampere meter, and measured a current when the reactions were reversed.

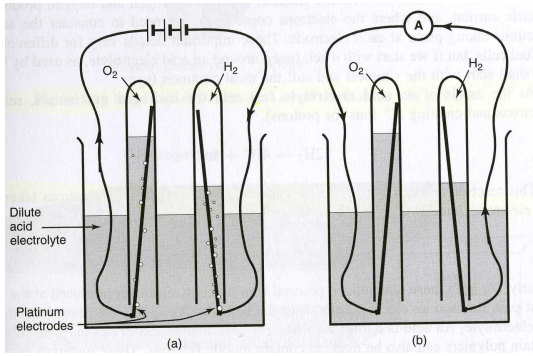

Figure 3.1: Schematic illustration of Sir William Grove's gas voltaic battery from 1839. In a) the cell is connected to an electrical power source, and electrolyzes water. In b) the power source is replaced by an ampereometer (or load), and it is now a crude fuel cell. From [8].

The anode reaction in a hydrogen fuel cell is as given in (3.2).

$$H_2(g) \rightarrow 2H^+ + 2e^-, E_a^\circ = 0V_{SHE} \tag{3.2}$$

The cathode reaction is given in (3.3).

$$\frac{1}{2}O_2(g) + 2H^+ + 2e^- \rightarrow H_2O(g), E_c^\circ = 1.23V_{SHE} \tag{3.3}$$

The total reaction is the two combined, as given in (3.4).

$$\frac{1}{2}O_2(g) + H_2(g) \rightarrow H_2O(g), E^\circ = 1.23V_{SHE} \tag{3.4}$$

The cell shown in Figure 3.1 would perform poorly and only produce small currents. There are several reasons for this, but the most pronounced is the long distance the ions have to travel. The electrolyte, which is diluted sulfuric acid, has a rather large resistance towards ion mobility. There is also a very small electrode/gas/electrolyte boundary, limiting the area at which the electrode reactions happen.

A more conventional fuel cell (more precisely a PEM fuel cell) is therefore more similar to the one shown in Figure 3.2. Here the anode and cathode are made flat to allow for maximum contact with the electrolyte, porous to allow gas penetration and release of exhaust product water, and the electrolyte is as thin as possible to minimize the resistance towards ion mobility (transport of charges).

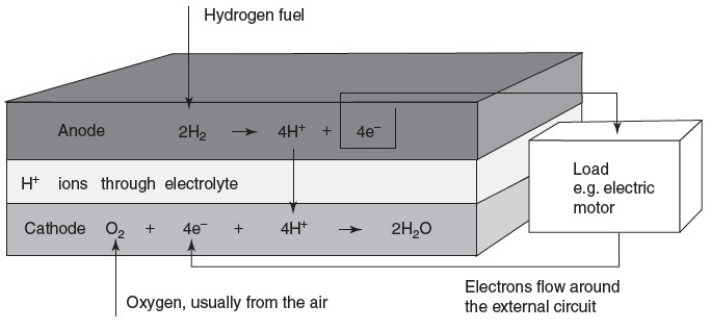

Figure 3.2: Schematics of a conventional proton exchange membrane (PEM) fuel cell. From [8].

The cell in Figure 3.2 has a solid polymer membrane as electrolyte (typically Nafion®), from which it derives its name; polymer electrolyte mebrane fuel cell (PEMFC). As mentioned in the previous section, PEMFCs have the advantage of fast response, solid electrolyte and moderate operating temperature. In addition it can use pressurized gas, and the cell itself can be subjected to a clamping pressure. A higher clamping pressure reduces the contact resistance for transferring electrons across the interfaces of the different parts of the fuel cell, and thus reduces the losses caused by electron transfer [9].

The efficiency losses in a hydrogen powered fuel cell are mainly connected to the activation over-potentials. This is a term for the energy barrier the reactions have to overcome in order to complete the charge transfer. This is countered by introducing active electrode materials for the reactions of interest (electrocatalysts) to lower the energy barrier, by raising the temperature or increasing the electrode surface area [8].

3.1.2 Water management in PEM fuel cells

Water is formed in the fuel cell reactions (see Equation 3.4) and also supplied by humidifying the feed gases into the fuel cell. Water is important since it

moists the membrane, and allows for transportation of protons [8]. It does however block the pores of the electrode or the gas diffusion layer, so excess water should be avoided. The case with too much water in the cell is called flooding of the cell, and reduces the efficiency of the cell by blocking the active sites of the catalyst. The opposite case, when the water content is too low, is called drying. This reduces the efficiency by inhibiting proton movement through the membrane.

Water management gets complicated by a number of factors. The electro-osmotic drag is the process where the protons travelling through the membrane drags with them between one and five water molecules. At high currents this could lead to drying of the anode side of the fuel cell.

The other main issue of water management is that when operating at temperatures above approximately 60 $^{\circ}C$ the air will always dry out the electrodes faster than water is produced.

The water management issues are solved by humidifying the feed gases into the fuel cell. To avoid flooding of the cell it is important that the excess water gets flushed out of the system. This is practically done by letting the air blow the water droplets that are formed out of the cell through the flow field channels.

3.1.3 Bipolar Plates

Oxygen/hydrogen gas has to be supplied to the electrodes continuously for the fuel cell to function. This is done by distributing the gas in small channels that keeps the GDL uniformly supplied with fuel. The useful voltage of a single hydrogen fuel cell is 0.7 V [8]. To obtain reasonable power output per fuel cell, several cells will have to be stacked in series. The bipolar plates are electrical conducting plates with flow fields on both sides. This facilitates gas distribution to both electrodes it is in contact with, in addition to connecting them in series. A sketch of a bipolar plate is given in Figure 3.3.

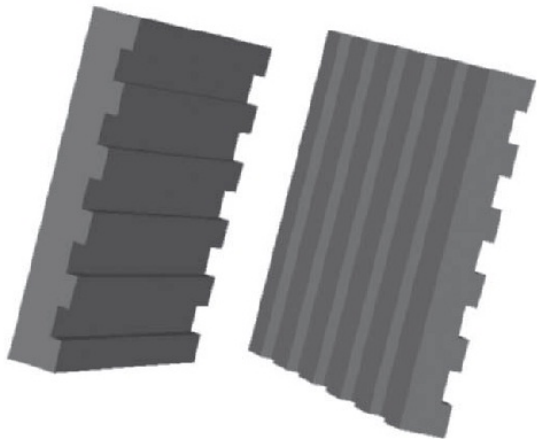

Figure 3.3: The left figure represent an endplate with flow field pattern on only one side (mono polar plate). The plate to the right represent a simple bipolar plate with flow fields on both sides. From [8].

To provide ideal electrical conductivity, the plates should have maximum contact with the electrodes, but this would inhibit the gas flow. It is therefore a weighed optimum of the size of the flow fields on the bipolar plates. The bipolar plates are expensive to produce, and in 2004 they amounted to about 11-45 % of the cost and 75 % of the weight of a fuel cell stack [14]. More recent numbers were not found, but it is expected the weight/cost fractions have dropped somewhat.

The American department of energy (DOE) has set some goals to be reached with respect to performance and cost for the bipolar plates for 2017 and 2020 [15]. A summary of the goals can be seen in Table 3.2.

Table 3.2: Requirements set by the American Department of Energy for 2017 and 2020 as well as 2011 status [15]

Characteristic	**2011**$_{status}$ [a]	**2017**	**2020**
Cost[b] $[\frac{\$}{kW}]$	$5-10$	3	3
Plate H_2 perm. coeff.[c] $[\frac{cm^3}{scm^2Pa}]$	N/A	$< 1.3x10^{-14}$[d]	$< 1.3x10^{-14}$[d]
Corrosion, anode[e] $[\frac{\mu A}{cm^2}]$	< 1	< 1	< 1
Corrosion, cathode[f] $[\frac{\mu A}{cm^2}]$	< 1	< 1	< 1
Electrical conductivity $[\frac{S}{cm}]$	> 100	> 100	> 100
Areal specific resistance[g] $[\Omega cm^2]$	0.03	0.02	0.01
Flexural strength[h] [MPa]	> 34	> 25	> 25
Forming elongation[i] [%]	20-40	40	40

a Status is based on information found in 2010 & 2011 Annual Progress Reports – project description write ups of TreadStone Technologies, Inc. and Oak Ridge National Lab.
b Costs projected to high volume production (500.000 stacks per year), assuming MEA meets performance target of 1000 mW/cm^2.
c Per the standard gas transport test (ASTM D1434), $80°C$, 3 atm 100%RH
d Blunk, et al, J. Power Sources 159 (2006) 533-542.
e pH 3 0.1ppm HF, $80°C$, peak active current $< 1x10^{-6}$ A/cm^2 (potentiodynamic test at 0.1 mV/s, -0.4V to +0.6V (Ag/AgCl)), de-aerated with Ar purge.
f pH 3 0.1ppm HF, $80°C$, passive current $< 5x10^{-8}$ A/cm^2 (potentiostatic test at +0.6V (Ag/AgCl) for >24h, aerated solution.
g Includes interfacial contact resistance (on as received and after potentiostatic test) measured both sides per Wang, et al. J. Power Sources 115 (2003) 243-251 at 200 psi (138 N/cm^2).
h ASTM-D 790-10 Standard Test method for flexural properties of unreinforced and reinforced plastics and electrical insulating materials.
i Per ASTM E8M-01 Standard Test Methods for Tension Testing of Metallic Materials

3.2 Coatings for Bipolar Plates

The environment inside a PEM fuel cell is acidic, with the pH of the outlet water ranging from 3.7 to 5, as well as fluorine levels of $10^{-5.5} - 10^{-3.5}$ [16]. This makes the interior of the fuel cell corrosive, and several solutions to the problem is being investigated. A brief overview of the currently used bipolar plate materials is shown in Figure 3.4.

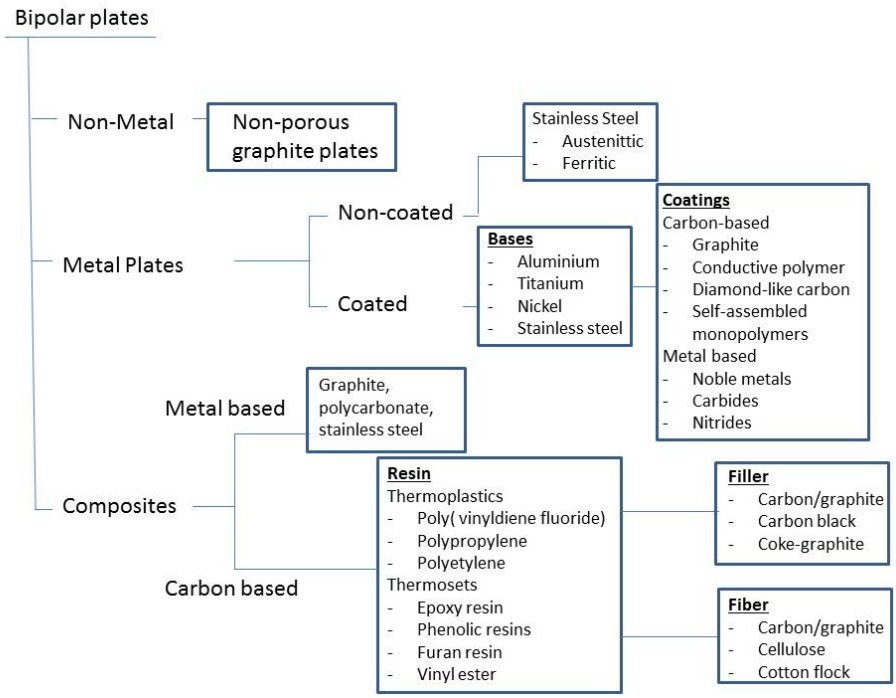

Figure 3.4: Common material choices for bipolar plates in PEM fuel cells. Adapted from [17].

The bipolar plates in Figure 3.4 all have strengths and weaknesses [17]. The graphite plates have good conductivities and are chemically stable (does not corrode). They are however brittle and difficult to machine, which makes them expensive and bulky. The stainless steel plates are cheap and easy to machine, but corrode inside the fuel cells. They therefore need to be coated with something to reduce/eliminate the corrosion. Gold coating works well, but is expensive so alternatives are sought after.

In this work we focus on metal based bipolar plates with carbon based coatings. Metal bipolar plates can easily be mass produced in various ways, the most common and cheap today is embossing (stamping) [18]. A coating achieving complete coverage might facilitate the use of a lower (and thus cheaper) steel quality.

For this work two different grades of steel has been used, 304 and 316L. The compositions of the alloys has some variation from vendor to vendor, but they should generally be within the range given in Table 3.3. Iron makes up the rest of the steel.

Table 3.3: Composition of alloying elements in the steel grades used in this work (wt %). Iron makes up the rest of the steel.

	C	Cr	Ni	Mn	Mo	Si	Ref
316L	<0.028	16.2-16.8	10.1-10.3	1.7-1.95	2.03-2.25	0.45-0.65	[19]
304	<0.08	18-20	8.0-10.5	<2	-	<1	[20]

3.3 Contact Resistance

The contact resistance is the resistance in the setup that can be attributed to the contact points between the different parts of the fuel cell. In this case it will refer to the resistance experienced over the contact area between the coating and the gas diffusion layer (GDL). In practice what is measured is the contact resistance over all interfaces.

The theoretical relationship between the contact resistance between a soft and a hard material and the compaction pressure is given by Spiegel et al. [21]. The relationship can be seen in (3.5):

$$R_C = \frac{A_a K G^{D-1}}{\kappa S^D} \left[\frac{D}{(2-D)p^*} \right]^{D/2} \tag{3.5}$$

In the equation above, R_C is the contact resistance [Ω m^2], A_a is the apparent contact area at the interface [m^2], K is a geometric constant [m], G is the topothesy (fractal parameter) of a surface profile [m], D is the fractal dimension of a surface profile, S is the scan length [m], p^* is the dimensionless compaction pressure and κ is the effective electrical conductivity of two surfaces [S m^{-1}], defined by (3.6):

$$\frac{1}{\kappa} = \frac{1}{2}\left(\frac{1}{\kappa_1} + \frac{1}{\kappa_2}\right) \tag{3.6}$$

Most of the parameters in (3.5) are constant, at least for the tests done in this work. The apparent area and the geometric constant are the same for all the plates tested (they all have the same size and geometry). The topothesy and the fractal dimensions are also expected to be fairly similar, as is the scan length. The conductivity of the coating does however to a large degree depend on the contents of the coating, and can not be expected to be constant from experiment to experiment. A simplyfied form of [3.5]

can therefore be expressed as (3.7):

$$R_C = \frac{C}{\kappa}(p^*)^{-\frac{D}{2}} \tag{3.7}$$

Where C includes all the constant parameters. For each of the experiments (at constant κ) it is now easy to see that the contact resistance is expected to decrease with increasing compression pressure. The drop is exponential with a rate of $-\frac{D}{2}$.

In the list of DOE's requirements to bipolar plates (Table 3.2), the goal for contact resistance is given with respect to a specified setup and experimental condition. This setup is the one developed by Wang et al. [19], and shown in Figure 3.5.

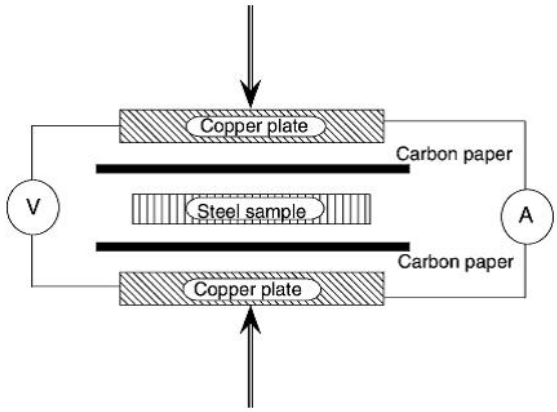

Figure 3.5: Contact resistance measurement setup as developed by Wang et al. [19].

The bipolar plate is placed in the center of the two copper plates, and a carbon fibre paper is placed on both sides. To find the contact resistance of a single BPP/GDL, the results are halved, and this would give the contact resistance between the steel and the carbon paper. The contact resistance for the copper/carbon paper has been corrected for by pressing a single sheet of carbon paper between the plates, and subtracting the half of these results from the measurements.

3.4 Degradation Mechanisms for Bipolar Plates

3.4.1 Oxide Formation

The mostly used stainless steel in this work is a stainless steel of the type 316L. This steel contains substantial amounts of chromium to avoid corrosion. The chromium creates a protective chromium oxide layer on the surface of the steel. This layer inhibits corrosion, but it greatly increases the contact resistance of the bipolar plates. This is because chromium oxide is electrically insulating. A Pourbaix diagram for 316L stainless steel is shown in Figure 3.6. This shows the stability of chromium in water as a function of potential and pH of the solution [22].

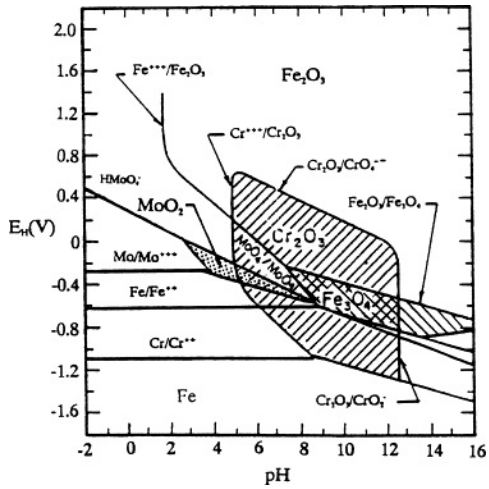

Figure 3.6: Pourbaix diagram for 316L stainless steel in water solution at 25 $°C$ [22].

The diagram shown gives an overly pessimistic view of the acid region, where the chromium oxide layer is expected to be unstable. The diagram is however based on thermodynamic data, and does not take into account the kinetics or bulk properties of the oxide. Stability of the layer in a H_2SO_4 solution up to 1 M has been shown by Yaniv et al. [23].

3.4.2 Carbon Corrosion

Graphite is a corrosion resistant material, and is often used in corrosive environments as substitutes for less noble metals. Carbon black (CB), which is else often used as catalyst support is however more reactive than carbon,

and can in some cases corrode. This is especially the case when using amorphous CB. More crystalline CB has less tendencies to corrode than amorphous [24]. The most prominent corrosion reaction is given in (3.8).

$$C(s) + 2H_2O \rightarrow CO_2 + 4H^+ + 4e^-, \; E_a^0 = 0.207V \tag{3.8}$$

Thermodynamically, carbon will corrode at potentials higher than 0.207 V vs SHE. The kinetics of the reaction is however slow, and severe carbon corrosion is not observed during normal fuel cell operation [24]. The rate of corrosion does however accelerate at abnormal conditions like shut downs or start-ups. An XRD pattern of different CB together with carbon nano tubes (CNT) and carbon nano cages (CNC) can be seen in Figure 3.7 (from Oh et al. [24]).

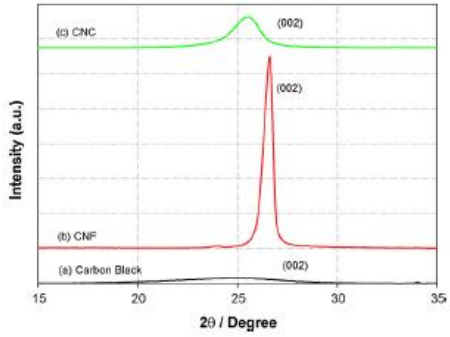

Figure 3.7: XRD pattern for Carbon Black, Carbon Nano Tubes (CNT) and Carbon Nano Cages (CNC) [24].

Both CNT and CNC have a higher degree of crystallinity than CB. Under a corrosion test taken at 1.4 V vs SHE for 30 minutes, the differences in corrosion as a function of crystallinity becomes evident. This is shown in Figure 3.8.

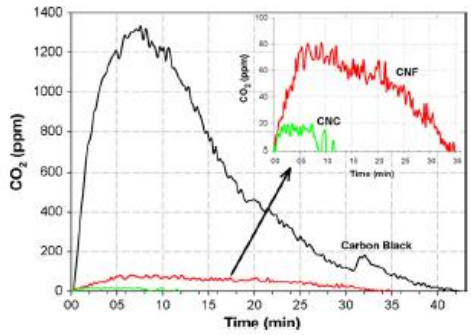

Figure 3.8: CO_2 mass spectra of MEA using Pt/CB, Pt/CNT and Pt/CNC catalysts, during corrosion test at 1,4 V for 30 min [24].

The mass spectra of CO_2 shows much more carbon corrosion for the carbon black based catalysts, than for the more crystalline carbon catalysts. This clearly shows that the amorphous carbon has a higher degree of corrosion than crystalline carbon.

3.4.3 Crevice Corrosion

The corrosion of iron and steel is highly dependent on the pH of the solution. Bockris et al. did kinetic studies on the deposition and dissolution of iron, and found that the corrosion current increases logarithmically with decreasing pH [25]. Their results are summarized in Figure 3.9.

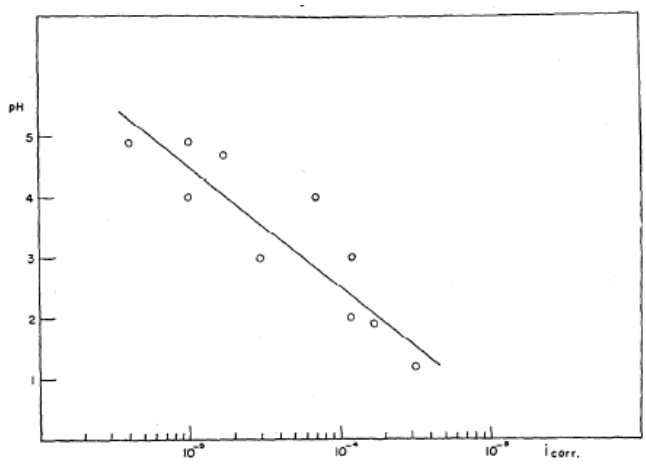

Figure 3.9: Corrosion current of iron plotted against pH of solution. From Bockris et. al [25].

If the metal substrate is covered by another material (in this work the carbon composite coating), crevice corrosion can occur in small cracks in the coating. In these small cracks, galvanic corrosion will at some point occur [26]. When galvanic corrosion starts, metal ions will be let into the electrolyte in the crevice, while the reduction occurs some other place. At some point the concentration of metal ions in the crevice will be high enough for formation of metal hydroxides. This will make the pH in the crevice drop by formation of H^+-ions according to equations (3.9) and (3.10):

$$Fe^{3+} + 2H_2O \rightarrow Fe(OH)_3 + 3H^+ \tag{3.9}$$

$$Cr^{3+} + 2H_2O \rightarrow Cr(OH)_3 + 3H^+ \tag{3.10}$$

As the pH drops, the corrosion current increases as seen in Figure 3.9. Small defects in the coating can therefore be the source of severe corrosion problems for the bipolar plates.

3.5 Scanning Electron Microscopy (SEM)

A scanning electron microscope works much like a light microscope, but instead of light, electrons are used to form an image. An electron beam is targeted at the sample, and interacts with the atoms in the sample. The energy of the electrons generated is usually in the range of 0.2 keV to 40 keV. When the electrons from the electron beam hit the sample, the atoms respond differently, and any diversities are picked up by the detectors [27]. The most common modes of operating a SEM is either to use the secondary electrons (SE) or to use backscattered electrons (BSE) detectors.

Secondary electrons are created when the electrons from the electron beam ionizes an atom. The incoming electron knocks off an electron from the atom, and it is usually in the range of 50-100 eV. The emitted electrons are then detected by a secondary electron detector, and an image of the surface can be acquired.

3.6 Contact Angle and Wetting

When a liquid drop comes in contact with a solid surface it will wet the surface to some degree. The wetting of the surface can be expressed in terms of contact angles [28]. At the surface of the solid a three phase boundary will be established between the solid, the liquid and the gas. The interfacial tensions of the solid and liquid boundaries is related through Young's equation (3.11).

$$\gamma_L \cdot \cos\theta = \gamma_S - \gamma_{SL} \tag{3.11}$$

In the equation γ_i denotes the interfacial tension of the liquid surface (L), the solid surface (S) and the solid liquid interface (SL). θ is the contact angle. If the solid interface has a higher tension than the solid-liquid interface ($\gamma_S > \gamma_{SL}$), $cos\theta$ had to be positive and the contact angle is higher than 90°. The liquid is then said to wet the solid. If the solid interface has a lower interfacial tension than the solid-liquid interface ($\gamma_S < \gamma_{SL}$), $cos\theta$ is negative, and the contact angle is greater than 90°. The liquid is then said not to wet the solid. A sketch of the two situations is shown in Figure 3.10 .

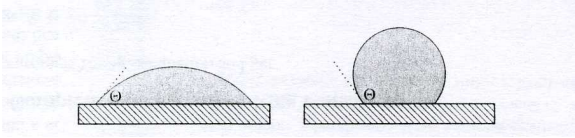

Figure 3.10: Wetting situation for a drop on a planar solid surface. Left shows a wetting drop (θ <90 °), and right shows a non-wetting drop (θ >90 °). Adapted from Butt, H. et al. [28]

.

Although Young's equation is used extensively to quantify wetting, it is not well founded and has not been verified experimentally. The main problem is related to determining the surface tension of the solid and the solid-liquid boundary . Another problem is that experimentally only advancing or receding contact angles can be determined. This means one can only define a range for the equilibrium contact angle.

Young's equation is also only valid for macroscopic scale (0.1-1 μm from the wetting line). Close to the wetting line the situation becomes more complex, as the surface forces can change the shape of the drop. The wetting of the surface can be used to determine the corrosion resistance of a material with or without a coating.

The roughness of the surface also plays a vital role in the wetting properties of the material. The effect of surface roughness can be described by the Wenzel equation (3.12):

$$\cos\Theta_{app} = R_{rough}\cos\Theta \tag{3.12}$$

Here Θ_{app} is the apparent contact angle which we observe. R_{rough} is the ratio between the actual and projected surface area. From this we can conclude that $R_{rough} \geq 1$. This in turn implies that low contact angles (Θ <90 °) will appear even lower, and high contact angles (Θ >90 °) appear even higher. A hydrophobic surface will therefore become even more hydrophobic by roughening the surface. By making microscopic, hydrophobic spikes, it is possible to create a super-water-repellent surface. This is called the lotus effect, because the lotus leaves utilize this phenomena to create a surface water repels from and takes with it dirt particles, keeping the surface clean.

The inhomogeneity of the surface also plays a role in the hydrophobic character of the material. If there is two regions on the surface (Θ_1 and Θ_2) which covers the surface ratio of f_1 and f_2 the apparent contact angle can be calculated by using the Cassie equation (3.13):

$$\cos\Theta_{app} = f_1\cos\Theta_1 + f_2\cos\Theta_2 \tag{3.13}$$

Since the coatings in this work will be tested in an electrochemical cell, also the electrowetting phenomena might have to be considered. An illustration of the electrowetting phenomena is given in Figure 3.11

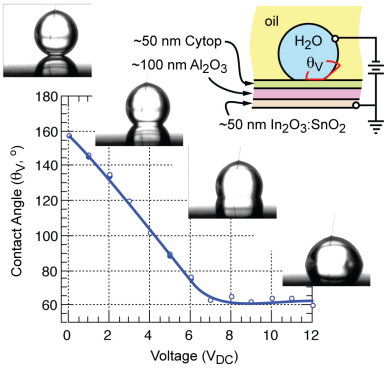

Figure 3.11: Electrowetting phenomena between a water droplet and a insulating layer on a metal surface, from [29].

The effect of electrowetting is however small at the limited potentials utilized in this work, and the effect is therefore neglected. The surface is also (at least partly) covered by conductive material, and this would not have the electrowetting effect.

Emel'yanenko et al. [30] did wetting experiments with a 0.5 M NaCl solution on bare low-carbon steel and on low-carbon steel coated with magnetite. They also did wetting experiments on a dense monolayer of hydrophobic fluoroxysilanes and a superhydrophobic nanotextured layer of fluoroxysilane. They found the contact angles of the droplets of 0.5 M NaCl to be steadily decreasing on the pure and magnetite coated steel. This was attributed to the surface changes that occur during corrosion. For the hydrophobic coated steel, there was no sign of corrosion within the first hours of contact. There was however a slight but continuous decrease in the contact angles, and this was attributed to diffusion of water through the coating defects. The superhydrophobic layer maintained contact angles exceeding 150 ° for many days. No signs of change in shape or signs of corrosion was observed after 3 days of contact.

Fu et al. [31] made a Ag-polytetrafluoroethene (Ag-PTFE) composite to achieve a hydrophobic, conductive coating on bipolar plates. They found the coating had less defects than the pure Ag coating (approx. 20 defects mm^{-1} vs. approx. 40 defects mm^{-1}). The coating also became smoother, giving a lower contact resistance at high pressures due to the larger contact area. The corrosion resistance was however not significantly altered by the PTFE additions. The amount of PTFE added was not given in the paper.

Blunk et al. [32] has applied for a patent with the title: "Stable ultralyophobic coating for PEMFC bipolar plate water management". Here they propose to use thin fluoropolymer coatings to achieve a hydrophobic surface on the bipolar plates to get better water management. They claim to have achieved static contact angles of between 90 ° and 120 ° with a coating thickness of less than 1 micron. The coatings remained hydrophobic after 162 days in hot water (80 $°C$), which shows good thermal and chemical resistance. The substrate materials were gold or carbon coated stainless steel.

3.7 Previous Work Done in This Group

The previous work done in this field by the research community in Trondheim (SINTEF, NTNU and HiST) has been documented in the master thesis's of Sigrid Lædre [7] and Hans Husby [6], as well as in a project work conducted during the autumn of 2012 by the author of this report [11].

Lædre [7] investigated the use of stainless steel as a material for bipolar plates. This was done by polarization experiments on the plates, both with coatings (gold and "coating A") and without coating. The experiments were conducted in sulfuric acid with different molarities and additives. She also did interfacial contact resistance measurements (ICR) on the plates before and after polarizing to see how the oxide layer changed during polarization. Gold coated plates were the only ones found to satisfy the DOE's goal on ICR performance. The plates coated with "Coating A" showed little increase in ICR after polarizing, but were above the goals set by DOE.

Husby [6] coated bipolar plates by air brushing epoxy with added graphite and carbon black (CB) onto the plates. The coatings were made with different formulas, and the plates were dried at elevated temperatures. Some of the plates were hot pressed at 1210 N cm^{-2} to achieve lower porosity. A novel concept of gluing the coated bipolar plates to the gas diffusion layer (GDL) was also developed. The most promising results was the hot pressed plates that achieved a contact resistance of 9.8 mΩ cm^2 at a compaction pressure of 125 N cm^{-2}. The plates that were glued onto the GDL had ICR results of 21.3 mΩ cm^2 at this same compaction pressure.

The paint that was developed is the same base composition that is being used in this work. It consisted of 45 vol % graphite, 5 vol% CB and 50 vol% epoxy. More details on the composition are given in the experimental section of this report.

In reference [11] from 2012 it was concluded that high pressure in the hot press produced coatings with low contact resistances. The best results were obtained by pressing the plates at 2043 N cm^{-2} at 110 $^{\circ}C$ for 3 hours which yielded a contact resistance at 150 N cm^{-2} of 8.46 mΩ cm^2. The low contact resistance was retained after linear sweeping the plates between -0.34 V and +0.76 V (vs. SHE) with a sweep rate of 2 mV s^{-1}. Other conclusions were that a compression time of 30 minutes is needed in the hot press to achieve minimal porosity, and longer compression times does not seem to give a better result.

Gold plates were tested in the contact resistance apparatus to determine the contact resistance in the GDL/gold interface. The real contact resistance between the coating and GDL is the measured contact resistance minus the gold/GDL contribution (Section 4.2, equation 4.2). The contact resistance for the gold plate tested is given in Figure 3.12

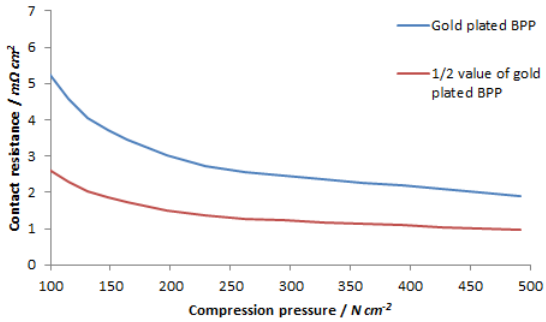

Figure 3.12: Contact resistance on gold plated bipolar plates (500nm from impact coatings) and the halves of the values.

The measured value 3.6 mΩ cm^2 at a compaction pressure of 147 N cm^{-2} means the contact resistance for the gold/GDL interface is as low as 1.8 mΩ cm^2.

Contact resistances measured on coatings compressed with different hot pressures are given in Figure 3.13.

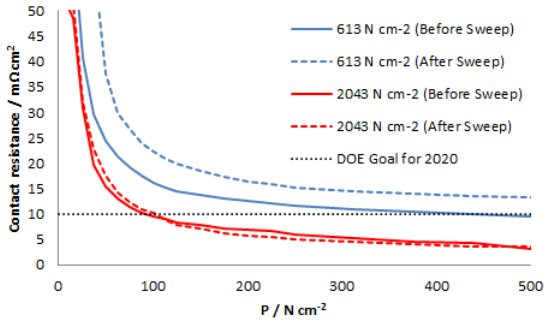

Figure 3.13: Contact resistance on coated stainless steel plates with a carbon based coating. The plates were pressed at 110 $°C$ for 3 hours.

3.8 Literature Review

3.8.1 Metallic Bipolar Plates with Carbon Based Coatings

Lee et al. [33] deposited CNT directly to 304SS sheets by catalytic decomposition of C_2H_2 using a tube furnace at atmospheric pressure. The sheets were afterwards covered with a polymer carbon composite. An interfacial contact resistance of 9.7 mΩ cm^2 was obtained for a compaction pressure of 200 N cm^{-2} for the best composition. Electrochemical measurements were taken in 1 M H_2SO_4 + 2 ppm F^- solution at 70 $^\circ C$ purged with H_2 and N_2. Potentiodynamic tests from -0.4 V to 1.0 V vs SCE (-0.156 V to 1.244 V vs SHE) at 2 mV s^{-1} revealed corrosion densities at -0.1 V and 0.6 V vs SCE below 1 μA cm^{-2}, which is the DOE goal [15]. Potentiostatic tests (3 h) also fulfilled the DOE goals.

Lee and Lim [34] painted 316L SS sheets with a polyamide-imide and CB slurry, dried them at 100 $^\circ C$ and then compression moulded the plates at temperatures between 200 and 320 $^\circ C$. ICR was measured as suggested by Wang et al. [19]. At 60 wt% CB, the contact resistance found its minimum at 25 mΩ cm^2 at a compaction pressure of 200 N cm^{-2}. Potentiodynamic tests were taken between 0.3 V to 1.0 V vs SCE at a rate of 1 mV s^{-1} in 1 M H_2SO_4 at 80 $^\circ C$. The minimum current density at 0.6 V vs SCE was found at 30 wt% CB to be 0.3 μA cm^{-2}.

Show [35] deposited a-C on Ti bipolar plates using radio frequency plasma enhanced chemical vapor deposition. The bare Ti bipolar plate had a contact resistance of 5.3 mΩ cm^2, while the coated plates obtained contact resistances down to 2.5 mΩ cm^2 with high deposition temperatures. The compaction pressure used was not given in the paper.

Show and Takahashi [36] applied a PTFE and CNT dispersion in water to a glass substrate or SS bipolar plate. Potentiodynamic tests were taken from the corrosion potential to 1800 mV vs Ag/AgCl for the coated SS plate. The scan rate was 5 mV s^{-1} and the electrolyte was 1 M H_2SO_4. The temperature was not given. The coated plate showed a passive current of 8 μA cm^{-2} at 600 mV vs Ag/AgCl. The interfacial contact resistance was given as 12 mΩ cm^2, but the compaction pressure was not given.

Fu et al. [37] prepared carbon-based films on 316L SS by pulsed bias arc ion plating. The C-Cr film showed a contact resistance of 6.86-8.72 mΩ cm^2 under 0.2-1.5 MPa (20-150 N cm^{-2}). Potentiodynamic tests were taken in a 0.5 M H_2SO_4 + 5 ppm F^- electrolyte at 25 and 70 $^\circ C$. For the measure-

ments, the scan rate was 2 mV s^{-1} from 0.1 V to 0.8 V vs SCE, and the current density was found to be about 0.1 μA cm^{-2}.

Yi et al. [38] deposited amorphous carbon onto a 0.1 mm thick 304SS foil using a CFUBMSIP system (closed field unbalanced magnetron sputter ion plating). The interfacial contact resistance is found to be 5.4 mΩ cm^2 at a compaction pressure of 150 N cm^{-2}. The wetting contact angle of the coated plate is found to be 78.8 °, while the bare 304SS gave a contact angle of 73.2 °. The angle was given as static.

Feng et al. deposited a carbon film onto a 316L SS sheet using closed field unbalanced magnetron sputter ion plating. Potentiodynamic measurements were taken in 0.5 M H_2SO_4 with 2 ppm HF at 80 °C from -0.6 V to 1.2 V vs SCE. At the cathode operation potential of 0.6 V vs SCE, the current density was measured to be 1.85 μA cm^{-2}. The potentiostatic test done at the same conditions at 0.6 V vs SCE, the current density stabilizes at 2.4 μA cm^{-2}. ICR for the sheets were also measured, and found to be 10.2-5.2 mΩ cm^2 under 90-210 N cm^{-2}. After potentiodynamic testing this increased to 46.0-18.4 mΩ cm^2.

Chung et al. [39] applied a 1 μm thick layer of nickel onto a 304SS substrate, and then used CVD to to create a carbon film on top of this layer. Potentiodynamic tests were taken in an undivided three-electrode glass cell from -1.0 V to 2.0 V vs NHE at a rate of 10 mV s^{-1}. The solution used was 0.5 M H_2SO_4 and the reference electrode was Ag/AgCl. They determined the plates to be as corrosion resistant as pure graphite plates, but did not give any numerical values.

Wang et al. [40] made a pure graphite sheet by compressing expanded graphite and used a binder polymer (with CB) to attach the sheet to 316L SS plates. Potentiostatic polarization was performed in 0.5 M H_2SO_4 at 25 °C at potentials of -0.1 V and 0.6 V vs Ag/AgCl (sat.) for 72 h. In the anodic condition the current stays at ca. -7 to -12 μA cm^{-2}, and at cathodic condition it stays at ca. -0.5 μA cm^{-2}. Potentiodynamic tests were performed in the same solution from -0.4 V to 1 V vs Ag/AgCl (sat.) with a sweep rate of 10 mV s^{-1}. The plate get a current density of 0.7 μA cm^{-2} at cathodic potential and -2.48 μA cm^{-2} at anodic potential. The area specific resistance is higher than for the bare 316L SS sheets, but approaches it by adding carbon fibre to the polymer.

Mawdsley et al. [41] developed a carbon-composite coating for aluminium bipolar plates for PEM fuel cells. Oxide free aluminium can meet all the DOE bipolar plate targets (5) exept for corrosion resistance. A matrix of

acid-resistant fluoropolymer (EFTE, Fluon, Asahi Glass Co.) containing different conductive filler materials was examined. The filler materials were graphite (Superior Graphite LGB2025), LaB_6, $TiSi_2$, TiC, TiB_2 and CaB_6.

Potentiostatic measurements were taken of the coated samples simulating cathodic potentials (0.8 V vs. SHE) and anodic potentials (-0.2 V vs. SHE) for 24-48 hours. The electrolyte was 1 mM sulfuric acid with 0.1 ppm NaF (pH=3) purged with argon, and the reference electrode was Ag/AgCl. The temperature was given as 80 °C. The stable corrosion currents measured for the cathodic potentials were around 1 μA cm^{-2}, while the stable corrosion currents measured for the anodic potentials were around 11 μA cm^{-2}.

Kitta et al. [5] developed a metal separator (bipolar plate) with carbon/epoxy coating. They made the plates starting from a flat metal plate, which they coated with a 60 vol% JB-5 graphite/bisphenol A based epoxy mix. Then they made the flow fields with 70 vol% PAG-5 graphite in cresol-novolak epoxy resin. The epoxy and graphite was mixed in a planetary ball mill into a paste, and added to stainless steel plates by blade coating. The plates were dried at 100 $^{\circ}C$, and then hot pressed at 190 $^{\circ}C$ for 30 minutes with pressures varying from 2-10 MPa (200-1000 N cm^{-2}). To screen the resin for the ribs, a layer (0.5 mm) was placed on top of some of the coated plates. The contact resistances measured were 12.2 mΩ cm^2 for the protective coating, and 13.8 mΩ cm^2 with the additional rib layer at a compaction pressure of 1 MPa (100 N cm^{-2}).

Fukutsuka et al [2] coated Fe-based materials with carbon by plasma assisted CVD (chemical vapor deposition). ICR was measured in a setup with the sample in the centre covered by carbon paper on both sides. A 4-probe resistance meter (TSURUGA 3569) measured the resistance between the two gold coated plates that pressed the carbon paper and sample together with an applied compaction force of 100 N cm^{-2}. They measured the contact resistance of the coated stainless steel to be below 10 mΩ cm^2, while the uncoated samples (stainless steels and nickel steels) gave results from above 50 mΩ cm^2 to above 300 mΩ cm^2.

Nowak et al. [4] developed a hydrophilic and conductive coating consisting of 1,2-bis(triethoxysilyl)ethane combined with modified, hydrophilic carbon black. The coatings were applied on a gold coated or PVD (physical vapor deposition) carbon coated stainless steel. The coatings treated with phenyl-sulfonic acid or carboxylic acid showed negligible increase ($<$2 mΩ cm^2) in contact resistance when on a gold/PVD carbon coated stainless steel. The coatings are hydrophilic, and the contact resistance rapidly degrades due

to oxide formation if the underlying steel is not gold coated/PVD carbon coated.

Joseph et al. [3] electrochemically deposited polyanilin and polypyrrol (both conducting polymers) coatings to 304 stainless steel. The contact resistances obtained at 150 N cm^{-2} compaction pressure was approximately 120 mΩ cm^2 for polypyrrol, and 850 mΩ cm^2 for polyanilin. An uncoated stainless steel plate obtained 850 mΩ cm^2 in the same measurement, and a pure graphite plate obtained $\sim$ 80 mΩ cm^2 (both at 150 N cm^{-2})

3.8.2 Other Solutions

Ismail et al. [42] examined the contact resistance between a graphite bipolar plate and gas diffusion layers (GDL) with and without polytetrafluorethylene (PTFE) loading in a setup similar to the one encountered in a PEM fuel cell with flow fields in the bipolar plate and a gas sealing gasket. This had an effect since the gas sealing gasket had a lower compressibility than the GDL, and the experienced clamping pressure between the bipolar plate and the GDL were thus lower than the pressure measured over the entire setup.

The contact resistances were expected to be higher for higher loadings of PTFE. In the experiment there was however proved no connection between the PTFE loading and the contact resistance of the GDLs. This was believed to be caused by the gasket controlling the compression of the GDL. The unloaded sample (which had the lowest initial thickness of approx. 370 μm) therefore performed worse than the loaded samples (5-50 wt%) which had comparable and higher initial thickness ($\sim$ 400 μm). At a compaction pressure of 150 N cm^{-2} the unloaded sample was found to have a contact resistance of 50-80 mΩ cm^2. The loaded samples were measured to 8-18 mΩ cm^2, with a tendency for lower contact resistances for higher PTFE loading. This was attributed to the slightly thicker GDL caused by loading which in turn increased the compaction pressure between the GDL and the bipolar plate.

Turan et al. [43] investigated bipolar plates formed by either stamping or hydroforming of 316L stainless steel, and coated by physical vapor deposition (PVD) of TiN, CrN or ZrN in thicknesses of 0.1, 0.5 and 1 μm. The surface roughness of the plates was determined by using an optical profiler (WYKO NT1100, Veeco Instruments Inc.). The roughness was comparable for the uncoated plates formed by hydroforming or stamping. After PVD of

ZrN however, the surface roughness was 30 % higher for the stamped plates than for the hydroformed plates. This indicated a larger degree of plastic deformation with introduction of slip bands when stamping the plates.

The interfacial contact resistance (ICR) for the plates was shown to give lower contact resistances at thicker coatings for ZrN and TiN, while the opposite trend was observed for CrN. Thinner coatings provided less protection from corrosion than thicker coatings, and the ICR of the plates after corrosion experiments were worsened compared to the untested plates. TiN at 1 μm thickness gave the best results in the work, with little change in ICR after corrosion experiment, and ICR values of $\sim$ 10 mΩ cm^2 at 150 N cm^{-2}.

Makkus et al. [44] studied the contact resistances of different stainless steels at high and low compaction pressures after they had been in use as anodes or cathodes for 350 hours. At a high compaction pressure (30 barg / 300 N cm^{-2}), the contact resistances varied from 6-30 mΩ cm^2. At low compaction pressure (4 barg/ 40 N cm^{-2}) the contact resistances varied from 25-55 mΩ cm^2. In both cases the anodes performed better than the cathodes.

3.8.3 Patents

This section will give an overview of relevant patents in the field.

Abd Elhamid et al. [45] patented a polymer coating containing graphite and carbon black. The graphite and CB was milled with a binder, before it was sprayed onto the plate. The plates were then cured at temperatures up to 2000 ° F (1093 ° C). The patented coating and technique was reported to produce coatings with a contact resistance of less than 20 mΩ cm^2 at a compaction pressure exceeding 200 psi (approximately 140 N cm^{-2})

Blunk et al. [46] got a patent granted with the title: "Conductive and hydrophilic coating for PEMFC bipolar plate". The summary given is as follows: "An electrically conductive plate for fuel cell applications comprises a plate body having at least one channel-defining surface and an electrically conductive hydrophilic layer disposed over at least a portion of the channel-defining surface. The electrically conductive layer includes residues of a silane coupling agent and electrically conductive hydrophilic carbon."

Guiheen et al. [47] got a patent granted with the title: "Corrosion resistant coated fuel cell bipolar plate with graphite protective barrier and method of making the same". The summay given is as follows: "A corrosion resistant

coated fuel cell plate and method of making the same are embodied in a metal plate provided with a graphite emulsion coating and then a layer of graphite foil which is pressed over the coating. The graphite emulsion bonds the graphite foil to the metal plate and seals fine scale porosities in the graphite foil. Flow fields are formed by stamping the coated fuel cell plate.

Jeong et al. (Hyundai) [48] applied for a patent with the title: "Metal separator plate for a fuel cell having a coating layer comprising carbon particles dispersed in a binder resin and a production method therefor". The summary given is as follows: "The present invention provides a production method for a metal separator plate for a fuel cell which can maintain superior electrical conductivity and corrosion resistance without other adverse effects not just initially but even when used for an extended period of time under operating conditions involving severe vibration such as in a vehicle, which allows continuous production processing, and which allows high production efficiency. The production method for a metal separator plate for a fuel cell of the present invention is characterised in that it comprises: (a) a stage in which a base material made of a metal plate is made ready; (b) a stage in which the surface of the metal plate is subjected to acid cleaning; (c) a stage in which the surface of the acid-cleaned metal plate is coated with a composition comprising a binder resin, carbon particles and a solvent; and (d) a stage in which the metal plate, whose surface has been coated with the said composition, is dried at a temperature lower than the thermal decomposition temperature of the binder resin and higher than the boiling point of the solvent, and in which a coating layer, comprising carbon particles dispersed in a binder resin matrix, is formed on the surface of the metal plate; and these processes are carried out in a continuous process."

Chapter 4

Experimental

4.1 Preparation of Plates

To represent the bipolar plates, thin stainless steel sheets with a surface area of 3.5X3.5 cm and thickness of 0.1 mm were supplied by partners in the project (ElringKlinger AG). The steels used were 316L and 304.

To remove the chromium oxide layer on the surface of the plates, they were put in a 12.5 % HCl solution (approx. 3.65 M) for 15 minutes. Chromium oxide is electrically insulating, and therefore needs to be minimized prior to coating to achieve a low contact resistance between the steel and the coating. Afterwards the plates were cleaned in deionized water to remove any leftover chloride ions that could cause pitting corrosion. The plates were then air dried in room temperature and weighed.

The powders were weighed out and mixed by shaking. The amounts of powder in each batch varies, and a summary can be seen in Table 4.1. Xylene was added to the powder mix, together with both parts of the epoxy. The mixture was then shaken by hand for a few minutes, before an ultrasonic pin (Dr. Hielscher UP200H) was put into the mixture. The mixture was mixed by ultrasound for 5 minutes before the spraying process starts.

Table 4.1: Weight fraction of each ingredient in the paint mixtures.

Serie	Epoxy	Graphite	CB	Zonyl
1	0.47	0.49	0.05	-
2	0.36	0.37	0.04	0.23
3	0.39	0.41	0.04	0.15
4	0.44	0.46	0.04	0.06
5	0.61	-	-	0.39
6	0.72	-	-	0.28
7	0.88	-	-	0.12
8	1.00	-	-	-
9	0.47	0.49	0.05	-
10	0.36	0.37	0.04	0.23
11	0.39	0.41	0.04	0.15
12	0.44	0.46	0.04	0.06

The Zonyl powder used was purchased from Dupont and has the tradename "Zonyl MP1200 Fluoroadditive". It has an average particle size of 3 μm and 90 % <9 μm. The graphite particles used are KS6 and the CB is "Super P®Li", both supplied from Timcal.

The mixture was sprayed onto the plates using an air brush (MEEC Tools Air Brush) bought at the local hardware store (Store: Jula). The air brush was filled with one Pasteur pipette of paint which is sprayed onto the plates. The plates were then rotated 90 °, and the process was repeated. The rotation is important to minimize the effect of spraying angle on the finished coating. After the entire paint batch had been sprayed onto the plates, they were left to dry approx. 30 minutes. They were then put in a hot press (Carver Hot Press) and pressed for 30 minutes at 10 tons set pressure and 110 $^{\circ}C$. This correspond to a pressure of 2670 N cm^{-2} (for calculation see Appendix A.3)

Series 9-12 were glass blasted by the workshop prior to coating to increase the roughness of the plates. This was done in order to increase the adhesion of the coating to the plates so that it would stick throughout the electrochemical tests. The plates were put into a chamber where they were bombarded by glass particles with an average size of approximately 50 μm.

Images of the plates before and after glass blasting is given in Appendix A.8, Figure A.32 and A.33

4.2 Contact Resistance Measurements

The samples were put into an apparatus like the one shown in Figure 4.1. The apparatus in principle consist of two gold coated copper plates that can be pressed together with a variable pressure. A known current of 2 A was forced through the sample, and the voltage was adjusted automatically accordingly.

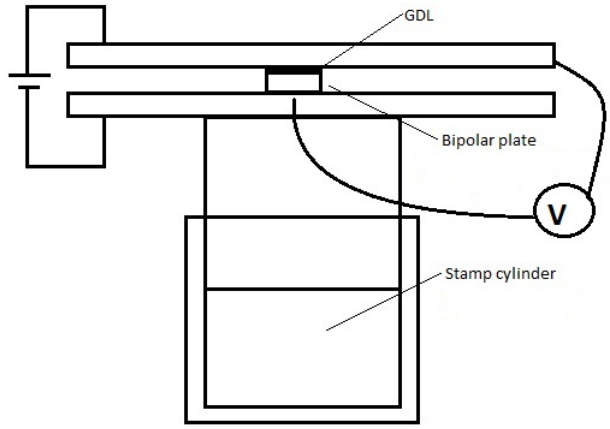

Figure 4.1: Setup of the interfacial contact resistance measurements

In the bottom plate a hole was drilled with a gold pin sticking out. An instrument measured the contact resistance between the top gold coated plate and the bottom pin. This contact resistance therefore includes the gold/GDL interface, the GDL/coating interface and the steel/gold pin interface as shown in (4.1).

$$\rho_{tot} = \rho_{gold/GDL} + \rho_{GDL/coating} + \rho_{steel/pin} \tag{4.1}$$

The contact resistance between the gold pin and the steel was assumed to be negligible due to the low area of contact, and the gold/GDL contact resistance was corrected for by withdrawing the contact resistance measured on a gold coated plate like shown in (4.2).

$$\rho_{measured} = \rho_{gold/GDL} + \rho_{GDL/gold} \Rightarrow \rho_{gold/GDL} = \frac{1}{2}\rho_{measured} \tag{4.2}$$

The plates were pressed together by increasing the pressure inside the piston of the apparatus (with nitrogen gas). Values for the contact resistances were manually recorded for the predetermined pressures.

The contact resistance measurement set-up described here was similar to the one suggested and described by DOE as reference setup (see Figure 3.5, developed by Wang et al. [19]). The main difference was that the set-up used in this work had a gold coated copper plate in contact with the GDL, to minimize the contribution to the contact resistance between the gold and GDL. A gold pin was used in this work to avoid any signal from the steel/gold interface on the uncoated side of the sheets.

Since the compaction pressure in the contact resistance apparatus is increased with fixed increments, the pressures read are fixed values. Even though DOE give their goals at a compaction pressure of 138 N cm^{-2} [15], the values in this work will be presented at 147 N cm^{-2} (the measured value closest to the recommended). This is to present a measured value and not an interpolated one.

A photography of the set up used is given in Appendix A.4, Figure A.1.

4.3 Electrochemical measurements

The plates will inside the PEM fuel cell experience a corrosive environment. The American Department of Energy has defined two test protocols for ex-situ testing of bipolar plate materials [15]. For simulating the cathodic environment, a linear sweep is suggested. For simulating the anodic environment, holding the plates at a given potential for a predetermined time is suggested. Both of the test protocols are described in the subsequent sections.

The set up used for the measurements is shown in Figure 4.2.

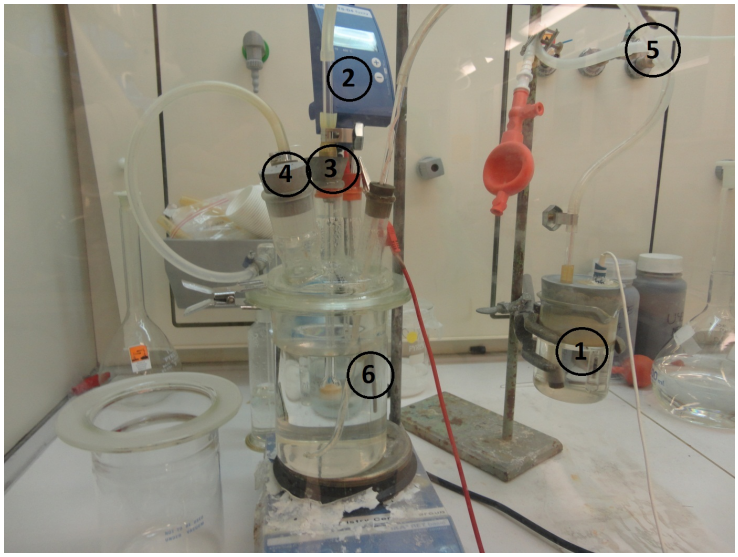

Figure 4.2: Three-electrode electrochemical cell for the corrosion simulation on the metal bipolar plates. 1. Reference electrode compartment with a $Hg/HgSO_4$ reference electrode. 2. Thermometer connected to the heating plate to control the temperature in solution. 3. Inlet for nitrogen-purge to remove oxygen in solution. 4. Entry point for the bipolar plates as working electrodes. 5. Custom made salt bridge connecting the working electrode chamber with the reference electrode chamber. 6. Counter electrode (Platinum foil).

To prepare the plates for electrochemical measurements, a platinum wire was welded onto the uncoated stainless steel backside of the plates. The backside was then coated with an electrically insulating lacquer, so that the signal obtained in the measurements was purely the coated side of the plates. The lacquer was applied using an airbrush in the same way described in section "4.1. Preparation of Plates". The lacquer is acetone thinned, so it was left to dry for some time before the plate was added to the setup. The plates had the role of working electrode.

All electrochemical measurements were done with an "GAMRY Reference 600 Potentiostat". The data was imported into a suitable data and graphical editing software.

4.3.1 Linear sweep

In this work we tried to get our experimental conditions comparable to the conditions suggested by DOE. For cathodic current measurements in solution with pH=3, 80 $°C$ and 1 ppm HF is suggested. The solution is to

be purged with argon gas to remove oxygen from the solution The voltage was swept from - 0.4 V to 0.6 V vs Ag/AgCl at a scanning speed of 0.1 mV s^{-1}. The potential of the Ag/AgCl reference electrode vs SHE is 0.223 V at 25 $°C$ [49], so this means a variation between -0.177 V to 0.823 V vs SHE. As a reference a $Hg/HgSO_4$ reference electrode was used, which has a potential vs SHE of 0.62 V [50]. To satisfy the goals set by DOE, the currents should be no higher than 1 μA cm^{-2}.

The tests conducted closely matched the conditions suggested, with a few exceptions. Firstly, a nitrogen purge was used instead of an argon purge. The results should however be compatible, because a removal of oxygen in electrolyte is obtained in both cases. Secondly, 1 ppm HF was not added to the electrolyte. This is partly to avoid the use of unwanted chemicals, but Lædre has also shown that fluorine addition $\leq$ 2 ppm does not alter the corrosion behaviour of stainless steel [51].

4.3.2 Chronoampereometry

The chronoampereometric tests was conducted in similar electrolyte to the one used in the linear sweep. The solution was however aerated (not purged with nitrogen). DOE [15] suggest a solution with pH=3, 80 $°C$ and 1 ppm HF, but the HF will not be added in this work with the same reasoning given in the previous section. The potential suggested is +0.6 V vs Ag/AgCl, and this corresponds to +0.823 V vs SHE. The test time suggested is >24 hours, but in this work 18 hours was used. This was due to a limited time frame for the work, and that the apparatuses were in use for other experiments.

4.4 Scanning Electron Microscopy (SEM)

SEM images of the samples were obtained with a "Hitachi S3400N" SEM to reveal the surface of the bipolar plates after coating in order to detect the dispersion of carbon within the epoxy, as well as any signs of cracks in the surface.

In this work the surface morphology is of interest and we expect no significant change in the surface composition. Consequently, all images are therefore obtained by the use of secondary electrons.

4.5 Scanning Light Microscopy (SLM)

A scanning light microscope (Alicona Infinite Focus) was used to get a measure of the surface roughness of the plates. This microscope scans in a line over the material, and at each point is focuses the image. The focused working distance can then be used to create a cross section of how the surface of the coating looks like. It also automatically calculates the roughness parameters of the coatings. The apparatus is shown in Figure 4.3.

Figure 4.3: "Alicona Infinite Focus" scanning light microscope.

The sample was placed beneath the objective lens, and the sample holder moved in a predetermined pattern, while the computer controlled the height of the lens and kept the image in focus. The movements of the lens was recorded, and this made an image of the surface.

The tests were taken with parameters that fulfil the 4287 and 4288 ISO standards. These are surface texture standards, and mostly regulates the distance the sweep should cover, and the number of points scanned in the sweep.

4.6 Contact Angle Measurements

Contact angle measurements were performed on the coatings to investigate the wetting of the coating. All the plates tested were firstly cleaned in deionized water, and afterwards dried in a heating cabinet set at 80 $°C$ for 30 minutes.

The apparatus used for contact angle measurements is an "Attension Theta

Lite Optical Tensiometer". An image of the apparatus can be seen in Figure 4.4.

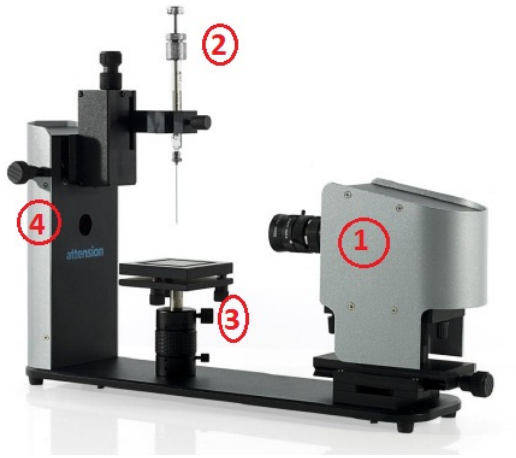

Figure 4.4: The Attension Theta Lite Optical Tensiometer. 1. Digital camera, 2. Syringe for placing drops, 3. Sample table, 4. Light source.

After cooling down to room temperature, a small drop was placed on the surface of the plate. The drop was placed using a syringe delivered with the contact angle measurement apparatus. A light source illuminated the drop from behind, and a camera recorded images of the drop. After defining for the software the base of the drop, it modelled the drop from the images using the Young-Laplace equation, and from this it calculated the contact angle. Measurements were taken on several locations of the sample, and the reported values are the average of the readings.

Since the drops slowly evaporated, the contact angle in each measurement decreased with time. To get comparable measurements, the images were therefore taken over a period of 10 seconds with a capture rate of 12 fps. The images were taken immediately after the drop had been placed on the plates.

For each plate two test were run, and the reported values are the average of the two.

Chapter 5

Results

This chapter will present the results obtained throughout the work.

5.1 Preparation of plates

When preparing the plates, the metal sheets were weighed both before and after coating. The measured difference in mass corresponds to the weight of the coating. By using the densities of the different components in the mixture, a theoretical coating thickness was calculated. The theoretical coating thicknesses obtained during coating is given in Table 5.1. The actual coating thicknesses is higher than the theoretical because of the porosity of the coatings.

Table 5.1: Theoretical thickness of the coatings prepared for this work (in μm).

Serie	Plate I	Plate II	Plate III	Average
1	13.47	11.56	11.20	12.08
2	42.24	28.34	25.99	32.19
3	13.17	11.66	15.82	13.55
4	25.41	24.18	26.47	25.35
5	21.80	13.69	13.60	16.36
6	30.40	20.46	27.53	26.13
7	7.14	6.32	7.14	6.87
8	13.16	10.07	8.42	10.55
9	36.02	29.61	31.79	32.47
10	18.28	22.05	21.23	20.52
11	44.00	49.24	48.75	47.33
12	48.52	59.51	63.95	57.33

The components in each of the series can be found in the Experimental chapter of the report (Chapter 4, Table 4.1).

5.2 Contact Resistance

Contact resistance measurements were taken to assess the charge transfer resistance of the boundary between the bipolar plates and the gas diffusion layer (GDL). These measurements were taken on the coatings containing carbon. The coatings consisting of only Zonyl (PTFE) and epoxy were not measured, as these were expected to be electrically insulating. Unless stated otherwise, the graphite, CB and epoxy content are constant (as given in the experimental chapter, 4).

5.2.1 Uncoated 316L Stainless Steel

As a reference to the results obtained by coating the stainless steel sheets, uncoated samples were tested before and after electrochemical measurements. Plates subjected to acid bath, for removal of any oxide layer (12.5 % HCl, 15 min) as well as as-delivered plates were tested. The resulting contact resistance measurement curves are given in Figure 5.1.

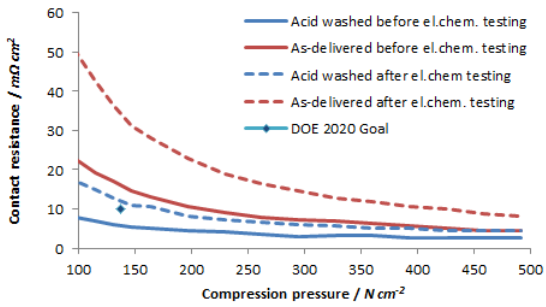

Figure 5.1: Contact resistance on acid washed and as-delivered uncoated 316L Stainless Steel sheets before and after electrochemical testing.

The acid washed stainless steel sheets achieved the goals set by DOE to be reached by 2020 in terms of contact resistance before electrochemical testing, but it increased after testing to values higher than 10 mΩ cm^2. The contact resistance at 147 N cm^{-2} was measured to be 5.5 mΩ cm^2 before electrochemical testing, and 11 mΩ cm^2 after testing.

The as-delivered sheets produces contact resistances above 10 mΩ cm^2 both before and after electrochemical testing. At 147 N cm^{-2} the contact resistance measured was 14.7 mΩ cm^2 before electrochemical testing, and 31.2 mΩ cm^2 after testing.

5.2.2 Coated Gold Plates

The coated gold plates supplied from one of the partners in the STAMPEM project was tested with a carbon composite coating (34.4 vol% graphite, 4 vol% CB, 13.2 vol% Zonyl and 48 vol% epoxy) of variable thickness. The contact resistances before and after the electrochemical testing is shown in Figure 5.2.

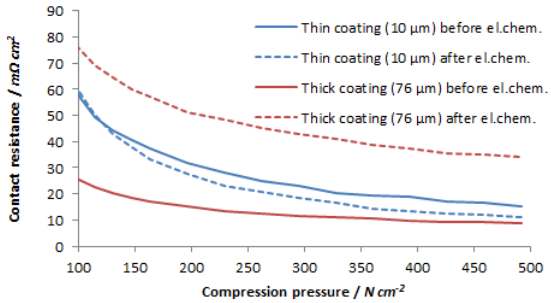

Figure 5.2: Contact resistance prior and post electrochemical measurements on gold coated 316L stainless steel plates with a coating consisting of 34.4 vol% graphite, 4 vol% CB, 13.2 vol% Zonyl and 48 vol% epoxy.

Before electrochemical measurements the thickest coatings produced the lowest contact resistance. The contact resistance at 147 N cm^{-2} was 18.4 mΩ cm^2 versus 40.4 mΩ cm^2 for the thickest coating. After electrochemical measurements the thinnest coating kept its contact resistance stable (in fact it is slightly lower than before), while the thickest coating got a substantial increase in contact resistance.

5.2.3 As-Delivered Plates

Before Electrochemical Measurements

Contact resistance dependence on the PTFE content was measured by making plates with different PTFE containing coatings. These were coated onto 316L stainless steel sheets that had been treated in 12.5 % (3.65 M) HCl for 15 minutes to remove the insulating oxide layer.

The resulting contact resistances measured for the sheets coated with varying amounts of added Zonyl in the coatings are given in Figure 5.3. A full overview of the results is given in Appendix A.4.

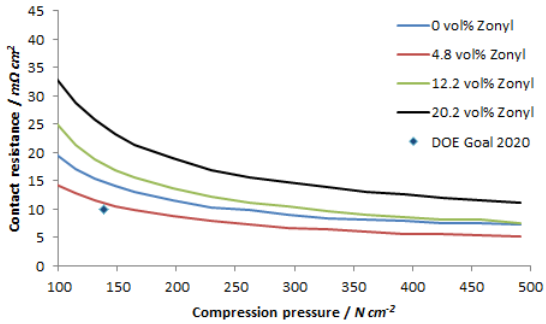

Figure 5.3: Contact resistance prior to electrochemical measurements on 316L stainless steel plates with Zonyl content in the coatings ranging from 0 vol% to 20.2 vol%.

For all concentrations of Zonyl in the coatings, the contact resistance decreased with increasing compaction pressure. The lowest contact resistance before electrochemical testing was achieved by the coating containing 4.8 vol% Zonyl. The other coatings got increasingly higher contact resistance with increasing Zonyl content.

None of the coatings acheived the DOE's 2020 goal for contact resistance, which is 10 mΩ cm^2 at a compaction pressure of 138 N cm^{-2} [15]. The coating with 4.8 vol% did however come close, with an average contact resistance of 10.6 mΩ cm^2 at 147 N cm^{-2}. One of the tests gave results as low as 9.2 mΩ cm^2. The coatings with 0 vol%, 12.2 vol% and 20.2 vol% resulted in average contact resistances of 14.1, 16.9 and 23.3 mΩ cm^2 respectively at a compaction pressure of 147 N cm^{-2}, all of which were much higher than the goals set by DOE.

After Electrochemical Measurements

The plates prepared without adding Zonyl lost their coating during the electrochemical measurements. The surface of the stainless steel was very smooth, and the adhesion between the plates and the coatings was a problem. This will be further presented in "5.3 Electrochemical Measurements" and in "6 Discussion".

Figure 5.4 shows two pictures of a coated plate without Zonyl before and after an 18 hour electrochemical test sequence was performed. From the pictures it is quite obvious that the coating peels off during the electrochemical test. The surface of as-delivered sheets is very smooth. In section

5.4 the smoothness of the plates is examined further.

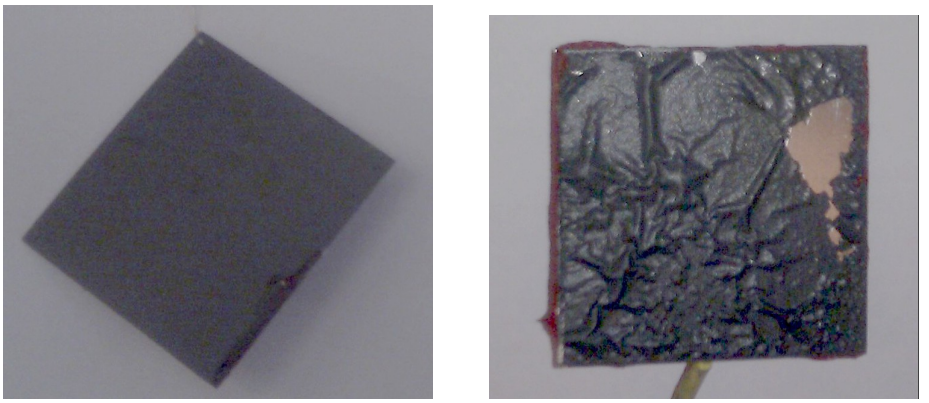

Figure 5.4: Stainless steel sheets coated with 40 vol% graphite, 5 vol% carbon black and 55 vol% epoxy. The plate before electrochemical testing is shown in the left figure, and the plate after electrochemical testing is shown in the right figure.

The coatings bloated up during the electrochemical testing, and when the coatings dried up afterwards it peeled of the plates. As the coating no longer adhered to the plates, the plates were not tested further in the contact resistance apparatus. The same problem occurred to most of the plates that were electrochemically tested.

For the plates with the coating with 20.2 vol% Zonyl content, the coating retained in 2 out of 3 tests. The contact resistance for the plates with the coating still intact is shown in Figure 5.5.

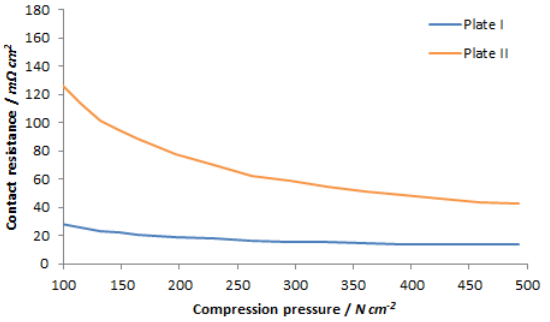

Figure 5.5: Contact resistance after electrochemical measurements on 316L stainless steel plates with 31.7 *vol*% graphite, 3.6 vol% carbon black, 20.2 vol% Zonyl and 44.5 vol% epoxy coating

The resulting contact resistance after potentiostatic testing ranged from 22 to 94 mΩ cm^2 at a compaction pressure of 147 N cm^{-2}. The latter of these is far above the goals set by DOE. The first value is around double the goal.

5.2.4 Glass Blasted Plates

Before Electrochemical Measurements

Since the coatings of the as-delivered plates peeled off during electrochemical measurements , plates were pretreated by glass blasting the surface to get a rough surface finish with more anchor points for the epoxy mixture. The composition of the coatings were identical to the ones used on the as-delivered plates.

The contact resistances measured prior to the electrochemical measurements are given in Figure 5.6. An expanded overview of all the results obtained is given in Appendix A.4

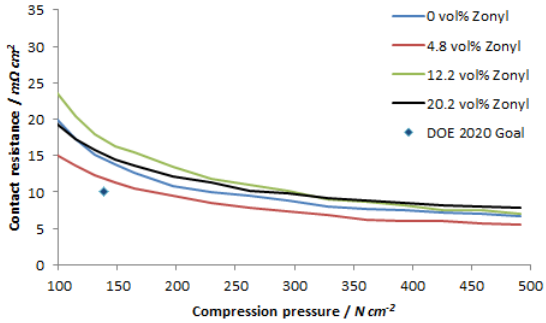

Figure 5.6: Contact resistance prior to electrochemical measurements on glass blasting 316L stainless steel plates with Zonyl content in the coatings ranging from 0 vol% to 20.2 vol%.

The coating with 4.8 vol% Zonyl produced the lowest contact resistance of all the coatings tested on glass blasted plates. The average contact resistance at 147 N cm^{-2} was measured to be 11.3 mΩ cm^2. One parallel produced a contact resistance at this compaction pressure of 10.4 mΩ cm^2.

The other coatings produced higher contact resistances. They ranked from lowest to highest contact resistance: 0 vol%, 20.2 vol% and 12.2 vol%. The numerical value for 0, 12.2 and 20.2 vol% Zonyl was 13.8, 14.5 and 16.2 mΩ cm^2 respectively at 147 N cm^{-2} compaction pressure.

Coatings were also applied to glass blasted 304 steel sheets to see if there were any differences from 316 sheets. The contact resistances measured before electrochemical testing are shown in Figure 5.7.

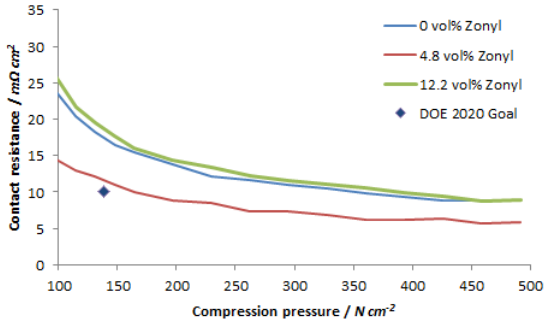

Figure 5.7: Contact resistance prior to electrochemical measurements on glass blasted 304 steel plates with Zonyl content in the coatings ranging from 0 vol% to 12.2 vol%.

The resulting contact resistances obtained on 304 grade steel were the same as was obtained using 316L stainless steel as substrate material. The lowest contact resistance obtained at 147 N cm^{-2} compaction pressure was 11 mΩ cm^2 for 4.8 vol% Zonyl in the coating.

After Electrochemical Measurements

For the glass blasted plates the adhesion proved a lot more resistant to the electrochemical tests. All of the coatings kept adhered throughout both the linear sweep and the 18 hour potentiostatic testing. The contact resistances measured after the electrochemical measurements are given in Figure 5.8. An expanded overview of all the results obtained is given in Appendix A.4

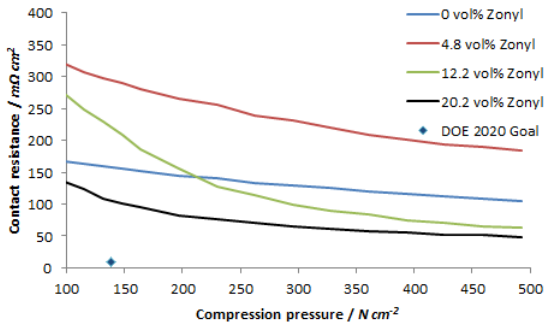

Figure 5.8: Contact resistance after electrochemical measurements on glass blasted 316L stainless steel plates with Zonyl content in the coatings ranging from 0 vol% to 20.2 vol%.

All the plates measured had a huge increase in contact resistance after electrochemical measurements. The best results were obtained for the coatings containing 20.2 vol% Zonyl, but even this result was 101.6 mΩ cm^2 at a compaction pressure of 147 N cm^{-2}. One of the plates in this series gave a contact resistance of 52.7 mΩ cm^2 at this pressure, but even this is over 5 times the goals set by DOE. The spread in the results were also more apparent in the measurements taken after the electrochemical tests, as can be seen in the more detailed graphs in appendix (A.4).

Plates with steel grade 304 were also tested electrochemically, and the contact resistance measurements after these tests are given in Figure 5.9.

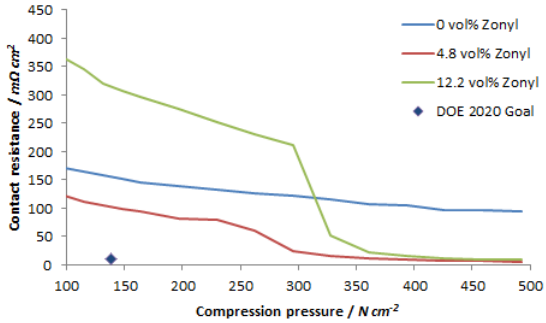

Figure 5.9: Contact resistance after electrochemical measurements on glass blasted 304 steel plates with Zonyl content in the coatings ranging from 0 vol% to 12.2 vol%.

All of the results are above the goals set by DOE to be reached by 2020. Both the coating with 12.2 vol% Zonyl and the one containing 4.8 vol% Zonyl experienced a pronounced drop between 250 and 350 N cm^{-2}. Both of the tests with drops in contact resistance were repeated, and the results were comparable.

5.2.5 Summary

A summary of the average contact resistances at 147 N cm^{-2} compaction pressure prior to electrochemical testing is shown in Figure 5.10

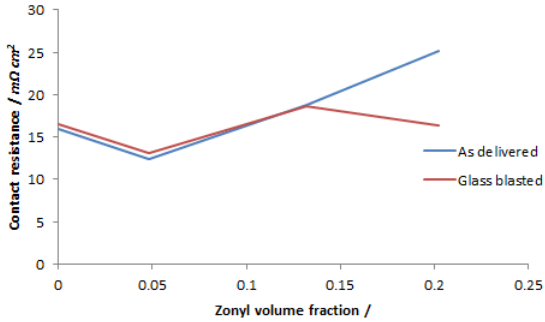

Figure 5.10: Contact resistance prior to electrochemical measurements on 316L stainless steel plates with coatings with differing Zonyl content. The contact resistance is taken at 147 N cm^{-2} compaction pressure.

The contact resistance decreases at small additions of Zonyl, but increases again as the Zonyl content was further increased. The trend was the same both for the as-delivered plates and the glass blasted plates. There was a small drop in contact resistance for the glass blasted plates at high Zonyl contents that is not seen for the as-delivered plates.

Figure 5.11 presents the connection between the theoretical thickness of the coating and the contact resistance.

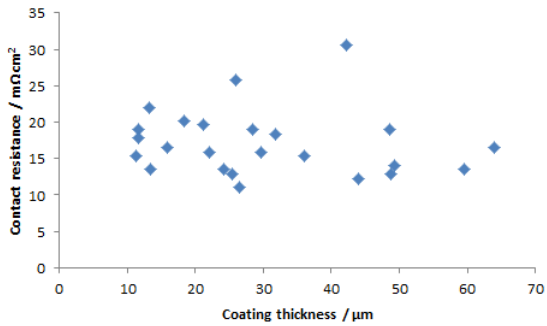

Figure 5.11: Contact resistance prior to electrochemical measurements on 316L stainless steel plates plotted versus the coating thicknesses. The contact resistance is taken at 147 N cm^{-2} compaction pressure.

There is no apparent trend in how the contact resistance is dependent on the coating thickness.

5.3 Electrochemical Measurements

The American department of energy has devised test protocols for ex-situ corrosion testing of the bipolar plates [15]. The details of the test protocol can be found in the experimental part of this report (4). Uncoated stainless steel sheets (316L) were tested both with and without removal of the oxide layer in 12.5 % HCl for 15 minutes, and provided reference data for the coated plates prepared in this work.

5.3.1 Dynamic Potential - Linear Sweep Voltammetry

Linear sweeps of the coated plates was conducted as described in the experimental chapter, section 4.3.1.

The numerical values for evaluating the corrosion currents of the coated plates is chosen to be taken at -0.1 V and +0.823 V vs SHE to be comparable to other work done in the field [33, 34, 36, 37, 40, 52, 53].

Uncoated 316L Stainless Steel Sheets

Uncoated stainless steel sheets were put through the same tests as all the coated samples. Figure 5.12 gives the current response from the linear sweep voltammetry measurements on both an as-delivered 316L stainless steel sheet and one acid washed as-delivered 316L stainless steel sheet.

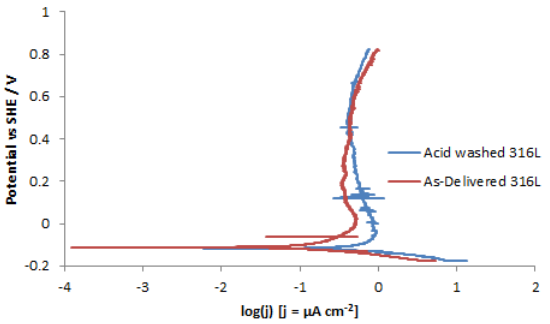

Figure 5.12: Linear sweep voltammograms of 316L stainless steel plates acid washed in 12.5 % HCl and without any prior treatment. The sweep rate used was 0.1 mV s^{-1}, and the electrolyte was 1 mM H_2SO_4 at 80 $°C$.

The current densities were low for both the scans, the current density at -0.1 V vs SHE was 0.11 μA cm^{-2} for the as-delivered plates, and 0.54 μA cm^{-2} for the acid washed plates. The current density was kept below 1 μA cm^{-2} throughout the scan (except for the small area in which hydrogen evolution occurs, see Appendix A.2. This fulfilled the goals set by DOE [15].

Coated Gold Plates

Linear sweep voltammetry was conducted on gold coated stainless steel plates covered with a carbon composite coating. The resulting voltammograms are given in Figure 5.13.

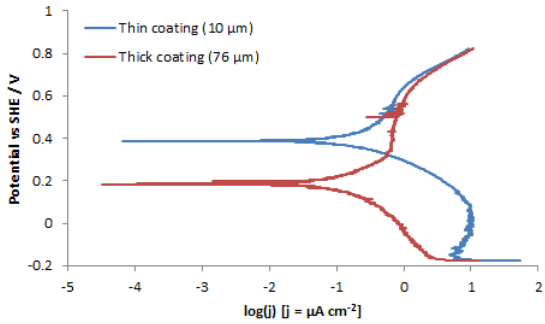

Figure 5.13: Linear sweep voltammograms on gold coated 316L stainless steel plates with a coating consisting of 34.4 vol% graphite, 4 vol% CB, 13.2 vol% Zonyl and 48 vol% epoxy. The sweep rate used was 0.1 mV s^{-1}, and the electrolyte was 1 mM H_2SO_4 at 80 $°C$.

The thick coating has a lower current density in the low potential range, but at higher potentials the current density is fairly equal for the two coatings. The coatings have current densities exceeding 1 μA cm^{-2}, and thus do not fulfill the requirements set by DOE for potentiodynamic current density [15].

Coated As-Delivered Stainless Steel Samples

Linear sweeps were performed on plates with varying concentrations of Zonyl. The resulting plots is given in Figure 5.14, along with the plot for uncoated 316L stainless steel. All of the plots recorded are given in Appendix A.5.

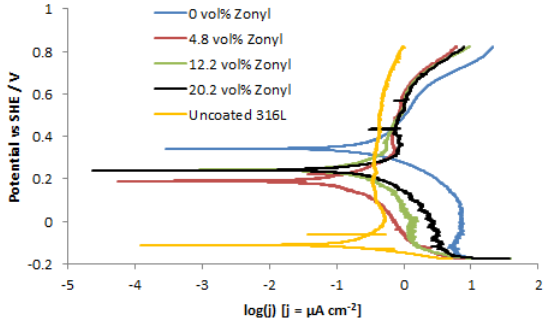

Figure 5.14: Linear sweep voltammograms on coated/uncoated 316L stainless steel plates with differing amounts of Zonyl. The sweep rate used was 0.1 mV s^{-1}, and the electrolyte was 1 mM H_2SO_4 at 80 $°C$.

The Zonyl containing coatings seem to perform better than the coating without any Zonyl. The uncoated stainless steel has a current density below 1 μA cm^{-2} in the entire potential range except the potential where hydrogen gas is evolved.

There is not much difference between the Zonyl containing coatings. The open circuit potential has small variations, but at the low currents present in the experiment, and varying oxygen concentrations, the OCP will be unstable anyway.

Coated Glass Blasted Stainless Steel Sheets

Linear sweeps were done on glass blasted 316L stainless steel plates with coatings with varying amounts of Zonyl. The resulting plots can be seen in Figure 5.15, and plots of all results are given in Appendix A.5.

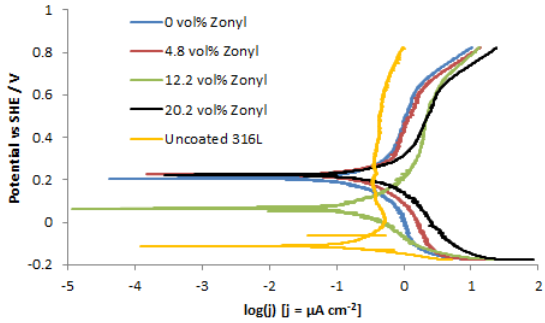

Figure 5.15: Linear sweep voltammograms on coated, glass blasted 316L stainless steel plates with differing amounts of Zonyl and a linear sweep on uncoated 316L sheets. The sweep rate used was 0.1 mV s^{-1}, and the electrolyte was 1 mM H_2SO_4 at 80 °C.

The current density measured increased slightly with increasing Zonyl content. All of the coatings gave current densities above the goals set by DOE to be reached by 2020 (1 μA cm^{-2}) [15]. There were some variations in the open circuit potential, where the coating containing 12.2 vol% Zonyl has an OCP some 150 mV below the others.

To see the difference in corrosion, 304 grade steels were also glass blasted and coated. The resulting linear sweep voltammograms recorded for these plates are given in Figure 5.16.

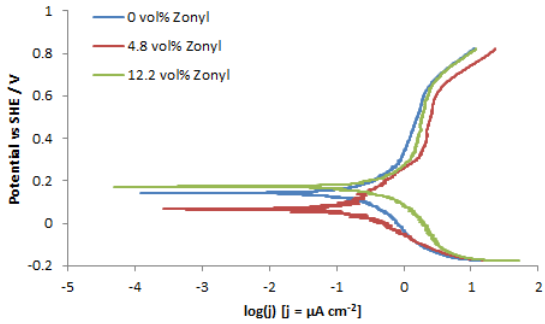

Figure 5.16: Linear sweep voltammograms of coated, glass blasted 304 steel plates with differing amounts of Zonyl. The sweep rate used was 0.1 mV s^{-1}, and the electrolyte was 1 mM H_2SO_4 at 80 $°C$.

The plots are similar to the ones obtained with 316L as substrate material (Figure 5.15), and the current densities were above the goals set by DOE for all the coatings. There was no apparent trend in the corrosion currents as a function of Zonyl content in the coating.

5.3.2 Static Potential

To simulate the cathode in the fuel cell, potentiostatic tests were done at 0.823 V vs SHE. The details of the test protocol can be seen in Chapter 4. This section will give an overview of the results obtained in this experiment.

Stainless Steel 316L

316L stainless steel plates both with and without the prior removal of the oxide layer were used as reference to the coated samples prepared in this work. The results are given in Figure 5.17

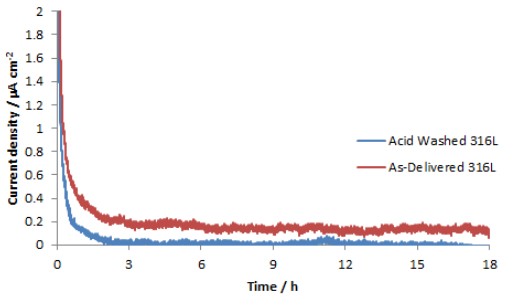

Figure 5.17: Chronoampereometric scan of 316L stainless steel plates acid washed and without any prior treatment. The test was taken for 18 hours at 0.823V vs SHE, and the electrolyte was 1 mM H_2SO_4 at 80 $°C$.

In both tests the current density rapidly dropped toward 0, and there was little current measured after 1-2 hours. Both the acid washed and the non-treated stainless steel samples tested fulfilled the goals set by DOE [15] (j <1 μA cm^{-2})

Coated Gold Plates

Chronoamperometric measurements were conducted on gold coated stainless steel plates with a carbon composite coating. The resulting plots can be seen in Figure 5.18.

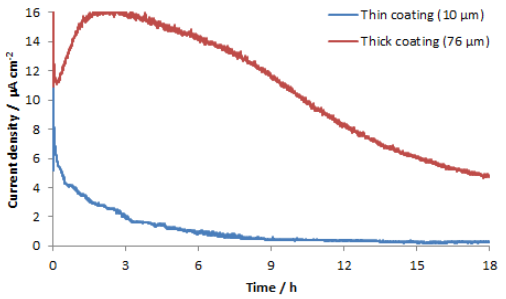

Figure 5.18: Chronoampereometric scans of gold coated 316L stainless steel plates with a coating consisting of 34.4 vol% graphite, 4 vol% CB, 13.2 vol% Zonyl and 48 vol% epoxy. The tests were taken for 18 hours at 0.823V vs SHE, and the electrolyte was 1 mM H_2SO_4 at 80 $°C$.

The thin coating stabilized at a current density of around 0.3 μA cm^{-2} and thus fulfilled the goals set by DOE [15]. The thicker coating got an increase in the current density, before it again drops. The current density ended up

around 5 μA cm^{-2}, but it seems the current density would have stabilized at a lower value if a longer scan had been conducted.

Coated As-Delivered Stainless Steel Samples

Potentiostatic measurements were done on carbon composite coated 316L stainless steel sheets with varying amounts of Zonyl in the coating. The resulting current densities are shown in Figure 5.19, and a summary of all measurements taken are given in Appendix A.6.

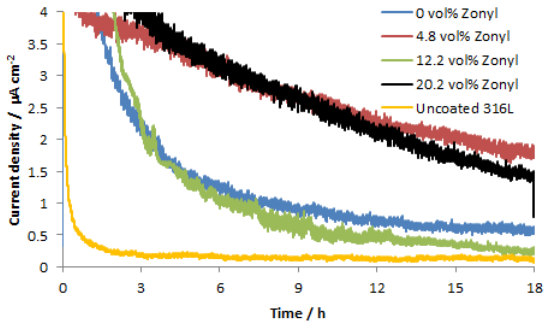

Figure 5.19: Chronoampereometric scan on coated/uncoated 316L stainless steel plates with differing amounts of Zonyl. The potential was kept at 0.823 V vs SHE for 18 hours, and the electrolyte was 1 mM H_2SO_4 at 80 $^\circ C$.

All the coatings produced current densities higher than what was the case for the uncoated stainless steel. The coating with 12.2 vol% Zonyl and the coating without Zonyl achieved the goals set by DOE for 2020 [15]. The coatings with 4.8 vol% and 20.2 vol% Zonyl was still a bit above the goals, but were still declining when the experiment was aborted. They still might have reached the goals set if the experiment had lasted longer.

Coated Glass Blasted Stainless Steel Samples

Glass blasted steel sheets were also coated, and the recorded current densities achieved in this experiment are shown in Figure 5.20. A more comprehensive overview of the results can be found in Appendix A.6. Note that the scale of the y-axis is different in Figure 5.19 and 5.20

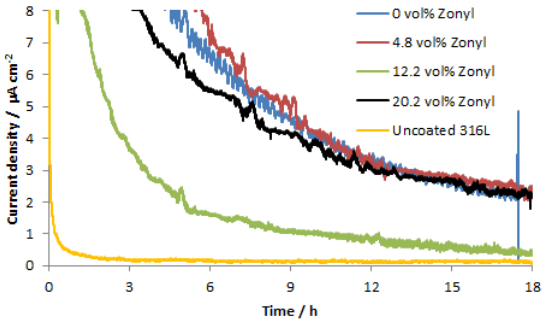

Figure 5.20: Chronoampereometric scan on glass blasted coated 316L stainless steel plates with differing amounts of Zonyl. Uncoated 316L sheets are also tested. The potential was kept at 0.823 V vs SHE for 18 hours, and the electrolyte was 1 mM H_2SO_4 at 80 $°C$.

The DOE targets [15] were fulfilled by the coating containing 12.2 vol% Zonyl. All the other coatings were around three times the value sought after at termination. However, the current densities continued to decrease towards the end of the experiment for all parallels indicating non-steady state behaviour, and a longer scan might lead to even lower current densities. Nonetheless, in this work we have assumed that 18 hours is sufficient to obtain steady state current densities.

To see the difference in corrosion behaviour on coated 316L stainless steel and coated 304 steel, 304 steel sheets were also glass blasted and coated. The recorded current densities are shown in Figure 5.21.

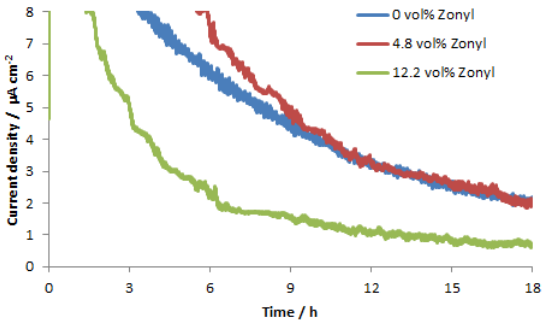

Figure 5.21: Chronoampereometric scan on glass blasted coated 304 steel plates with differing amounts of Zonyl. The potential was kept at 0.823 V vs SHE for 18 hours, and the electrolyte was 1 mM H_2SO_4 at 80 $°C$.

The coating with 12.2 vol% Zonyl achieved the goals set by DOE to be reached by 2020 [15], while the other coatings still produced too high cur-

rents. Yet again, the current densities of the other coatings were however still declining, and a lower steady state current density would have been achieved by longer scan times.

5.3.3 Summary

The correlation between the coating thickness and the current densities was recorded both at -0.1 V vs SHE from the potentiodynamic measurements, and at +0.823 V vs SHE from the potentiostatic measurements. The results from the potentiodynamic measurements are given in Figure 5.22.

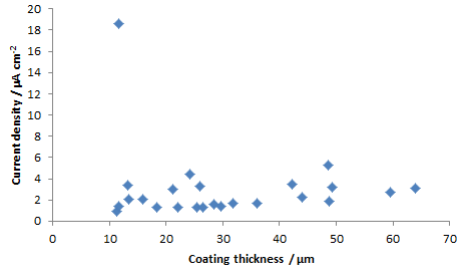

Figure 5.22: Current densities from the potentiodynamic measurements at -0.1 V vs SHE plotted against the coating thicknesses

The resulting current densities obtained from the potentiodynamic measurements shows no dependency on the coating thicknesses.

The results from the potentiostatic measurements are given in Figure 5.23.

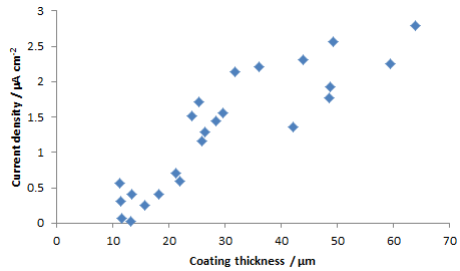

Figure 5.23: Current densities from the potentiostatic measurements at +0.823 V vs SHE plotted against the coating thicknesses

The current densities measured in the potentiostatic experiments increases with increasing coating thicknesses.

The effect of addition of Zonyl was investigated, and the average current densities from both potentiodynamic and potentiostatic measurements were plotted against the Zonyl content in the coatings. The resulting plots can be seen in Figure 5.24

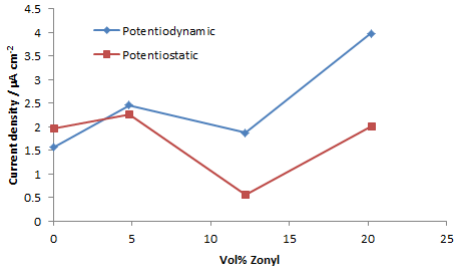

Figure 5.24: Current densities from the potentiostatic measurements at +0.823 V vs SHE and the potentiodynamic measurements at -0.1 V vs SHE plotted against the amount of Zonyl in the coating

There is no apparent trend in the current densities as a function of Zonyl content, although a small drop can be identified for both the potentistatic and potentiodynamic current density at 12.2 vol% Zonyl.

5.4 Scanning Electron Microscopy

Scanning electron images were taken of the surface of the coatings, before and after electrochemical measurements.

An image taken with secondary electrons of the coating without Zonyl is given in Figure 5.25

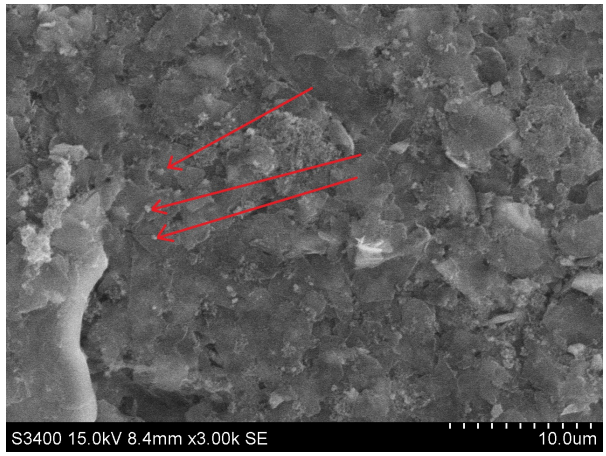

Figure 5.25: Scanning electron microscopy image of coating with 40 vol% graphite, 5 vol% carbon black and 55 vol% epoxy. The red arrows point at what is believed to be carbon black particles.

The surface of the coating has a smooth appearance, but with a closer look at the SEM pictures, the coating contains flakes of various sizes connected to each other quite tightly after hot-pressing at high pressure. The coating thus seems to be able to conduct electrons quite well, as there is little charging of the surface in the image. Small dots are scattered all over the coating surface, and this is probably the carbon black particles. This is indicated by the red arrows in the image.

An image of the coating with 20.2 vol% Zonyl is shown in Figure 5.26.

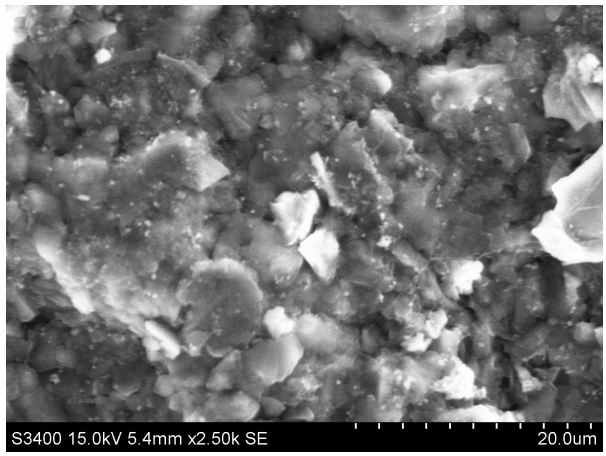

Figure 5.26: Scanning electron microscopy image of coating with 31.7 vol% graphite, 3.6 vol% carbon black, 20.2 vol% Zonyl and 44.5 vol% epoxy.

Similar dots as in Figure 5.25 can be observed here. There are more charged areas (white, blurry) in the image, which could be either of the electrically insulating components; epoxy or Zonyl. They do however seem to be evenly scattered, leaving a predominantly conductive surface. The SEM images for the other coatings can be found in appendix A.7.

Since the coatings peeled of the sheets during electrochemical measurements, and this had not been a problem in previous work in our laboratories, uncoated metal sheets were examined in the SEM and compared to images of the plates used previously. The resulting SEM images are shown in Figure 5.27 and 5.28.

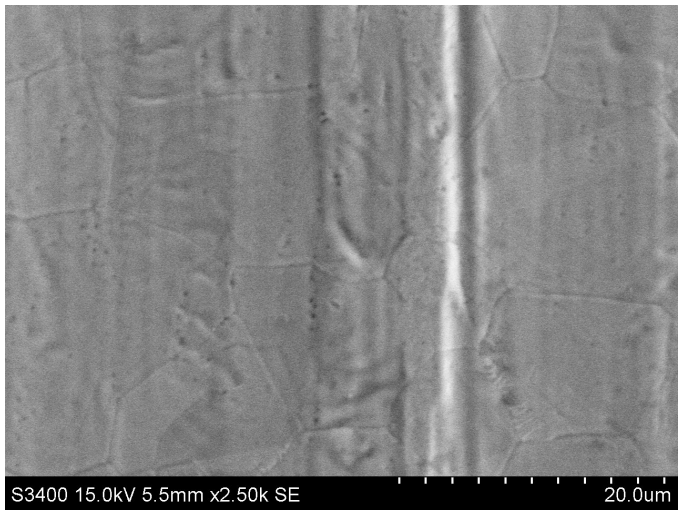

Figure 5.27: Scanning electron microscopy image of a new and smooth 316L stainless steel sheets.

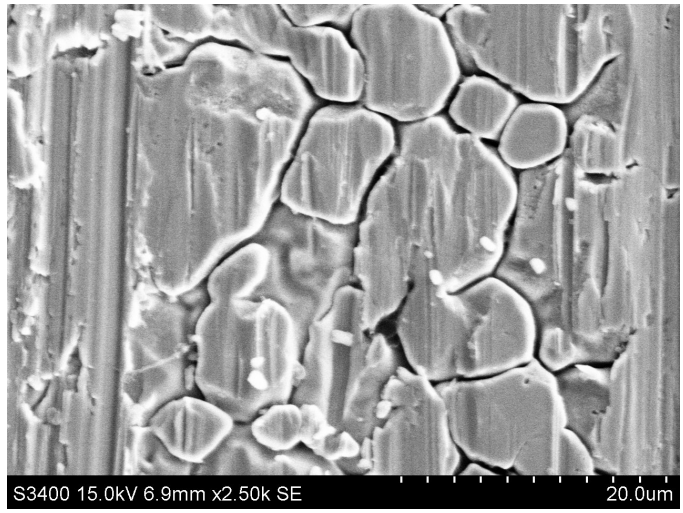

Figure 5.28: Scanning electron microscopy image of an old and rough 316L stainless steel bipolar plate used in previous work.

The images show that the morphology of the two stainless steel plates plates are very different. The plates previously used has a rough surface, while the newly acquired plates are very smooth. To roughen up the surface of the new metal sheets for better adhesion of the epoxy based coating, they were glass blasted. The resulting surface is shown in the SEM image in Figure 5.29.

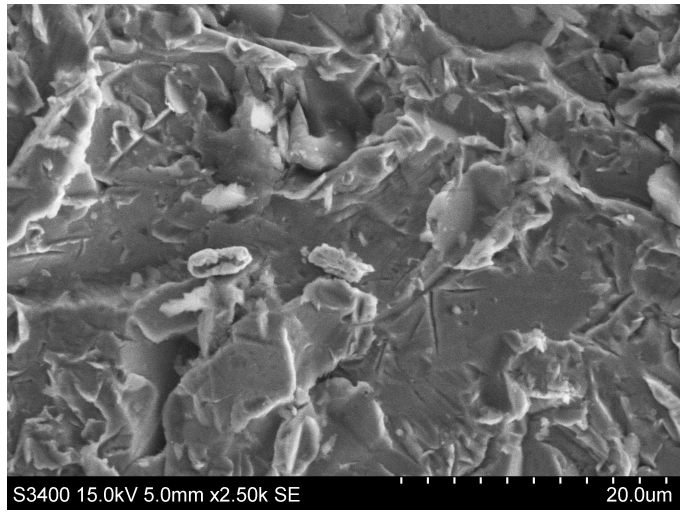

Figure 5.29: Scanning electron microscopy image of glass blasted 316L stainless steel sheets.

The glass blasted plates gave a much rougher surface, and resulted in a better adhesion of the coating.

On the glass blasted, coated plates images were taken both before and after electrochemical measurements. A coating with 4.8 vol % Zonyl is shown before electrochemical measurements (Figure 5.30) and after electrochemical measurements (Figure 5.31).

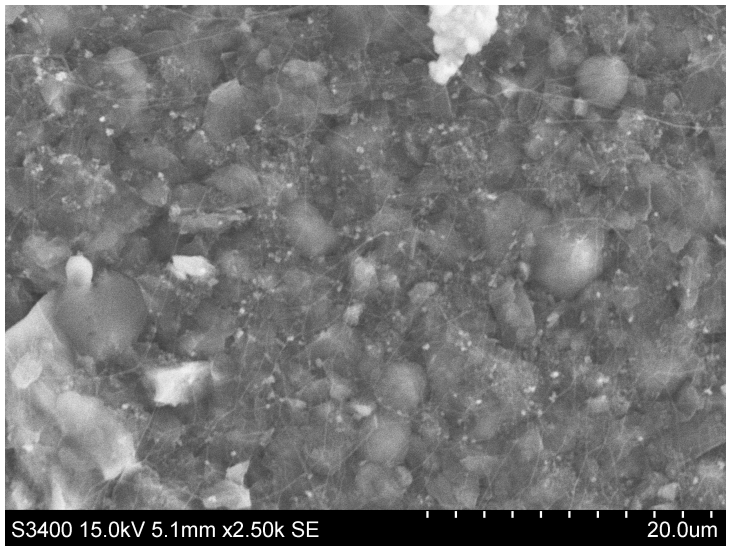

Figure 5.30: Scanning electron microscopy image of coating with 34.5 vol% graphite, 3.9 vol% carbon black, 13.2 vol% Zonyl and 48.4 vol% epoxy before electrochemical measurements.

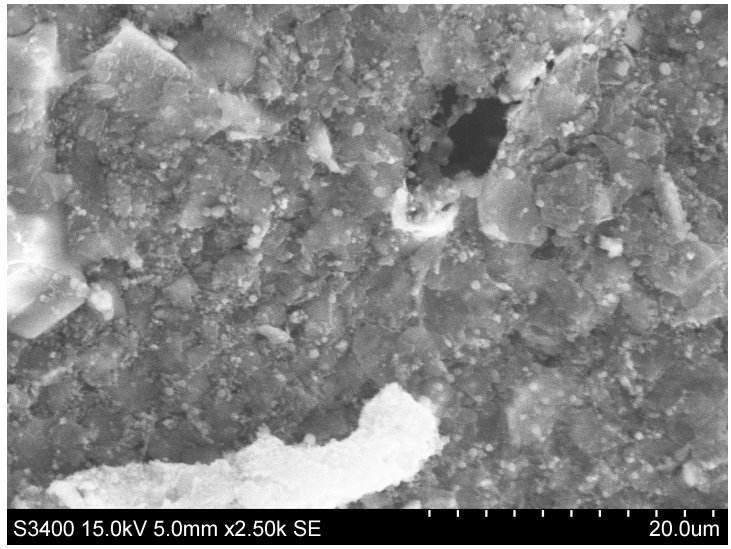

Figure 5.31: Scanning electron microscopy image of coating with 38 vol% graphite, 4.3 vol% carbon black, 4.8 vol% Zonyl and 53 vol% epoxy after electrochemical measurements.

Before the electrochemical measurements, small white thread-like lines can be seen, just like cracks in a thin ice layer. These seem to partially disappear after electrochemical measurements, but instead there are a lot more of the white spheres scattered all over the surface. The top layer, consisting of a thin layer of epoxy, seems to have been removed during the electrochemical measurements, while the carbon black has not been affected and now form most of the outer layer of the coating.

Also note the hole in the coating seen in Figure 5.31. It is difficult to measure the depth of such a hole in the SEM, but if it tunnels all the way down to the metal surface, this might facilitate corrosion processes of both carbon particles and steel.

5.5 Scanning Light Microscopy

Some of the coatings were characterized in a scanning light microscope, and the results are presented in this section.

The roughness profile of the coating without any Zonyl content is given in Figure 5.32

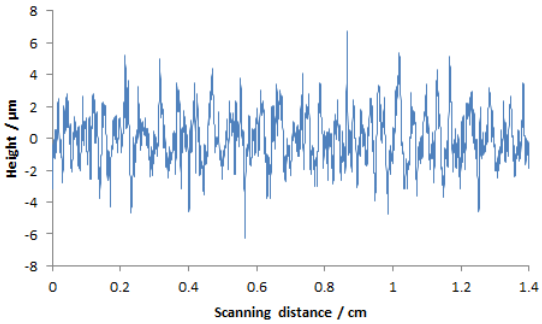

Figure 5.32: Scanning light microscopy roughness profile of coating with 40 vol% graphite, 5 vol% carbon black and 55 vol% epoxy.

The cross section shows a maximum offset from the mean of around 6 μm. The average roughness of the profile is calculated by the computer program used to acquire the data to be 1.48 μm. The mean peak to valley height of the roughness profile is calculated to be 13.85 μm.

The roughness profile of the coating with 4.8 vol% Zonyl content is given in Figure 5.33

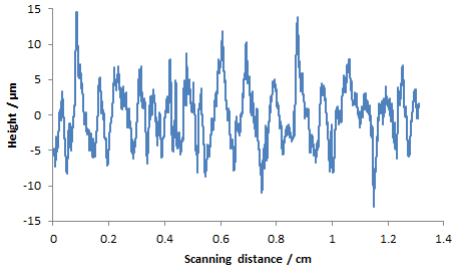

Figure 5.33: Scanning light microscopy roughness profile of coating with 38 vol% graphite, 4.3 vol% carbon black, 4.8 vol% Zonyl and 53 vol% epoxy.

The roughness profile indicated a maximum offset from the mean of around 14 μm. The computer program estimated the average roughness of the coating to be 3.16 μm and the mean peak to valley height to be 21.4 μm.

The profile of the coating with 13.2 vol% Zonyl content is given in Figure 5.34

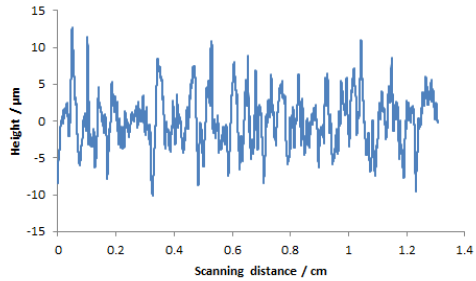

Figure 5.34: Scanning light microscopy roughness profile of coating with 34.5 vol% graphite, 3.9 vol% carbon black, 13.2 vol% Zonyl and 48.4 vol% epoxy.

The roughness profile indicated a maximum offset from the mean of around 12 μm. The computer program estimated the average roughness of the coating to be 2.99 μm and the mean peak to valley height to be 21.2 μm.

In both cases with Zonyl added, the average roughness was about double of the ”clean” carbon/epoxy mixture. The mean peak to valley height was also twice as high for the coatings with Zonyl. The amount of Zonyl in the mixture did however not significantly affect the roughness parameters.

5.6 Contact Angle and Wetting

Contact angle measurements were run on the coatings, and the results are presented in this section. The measurements were run for 10 seconds, with two parallels on each of the coatings.

The resulting contact angles as a function of the Zonyl content in coatings containing the standard amounts of graphite and CB is shown in Figure 5.35.

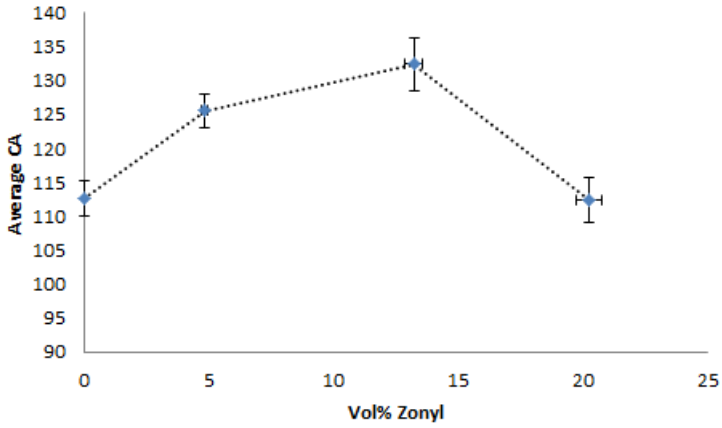

Figure 5.35: Contact angle measurements on coatings with graphite and carbon black as a function of the Zonyl content.

The contact angle increases with increasing Zonyl content up to a certain point, after which it again drops. As a result the hydrophobicity of the coatings seem to reach a maximum somewhere between 12.2 and 20.2 vol% Zonyl in the coating.

Contact angles were also measured on coatings without any graphite and carbon black. The results are presented in Figure 5.36.

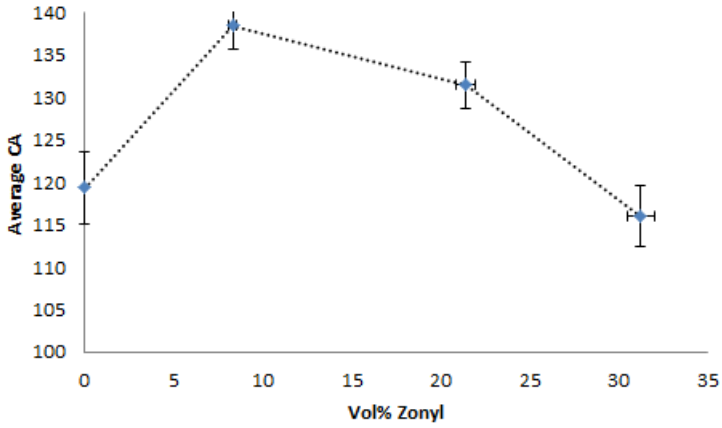

Figure 5.36: Contact angle measurements on coatings without graphite and carbon black as a function of the Zonyl content.

The contact angle increases with increasing Zonyl content at low concen-

trations, but at some point it decreases with increasing Zonyl content. The maximum hydrophobicity seems to be somewhere between 8.3 and 21 vol% Zonyl in the coating.

The hydrophobicity has a great effect on water droplet behaviour on the surface of the coating. The difference is easily seen when comparing two extremes of the coatings tested. In Figure 5.37 two droplets are shown. To the left a picture of a droplet on the coating without any Zonyl or graphite/CB is shown. The image to the right shows a droplet on a coating with 8.3 vol% Zonyl and no graphite/CB.

Figure 5.37: Droplets on coatings without graphite/CB. The left image is without Zonyl content, and the right image is with 8.3 vol% Zonyl.

The images show a large difference in the hydrophobicity, and this is consistent with the numeral values for the contact angles determined by the software.

Chapter 6

Discussion

6.1 Test Parameters

The coatings used are porous, and therefore electrolyte penetrates the coating and initiate oxide formation of the underlying stainless steel surface. This in turn increases the contact resistance between the plates and the gas diffusion layer. A number of attempts have been conducted to minimize the porosity, both in the previous project work [11] and in the master thesis work of Hans Husby [6]. The use of heat and pressure during curing of the coatings was shown to decrease the contact resistance significantly, and the coatings developed were close to the interfacial contact resistance goals set by the American Department of Energy (DOE) [15] to be reached by 2020.

The contact resistance apparatus used in this work differs somewhat from the apparatus described by Wang et al. [19] (the apparatus recommended by DOE). The main difference is that in our work we used a gold plated pin on the backside of the coated metal sheets instead of coating both sides of the metal sheet and measure the contact resistance over two GDLs sandwiching the sheet.

Using the pin made the contact resistance on the uncoated side of the plate negligible, since the contact area between the back plate and the pin was very small. The contact resistance measured was therefore almost exclusively the contact resistance between the coating/GDL and GDL/top gold plate.

DOE has also defined test routines for bipolar plate coatings for ex-situ test-

ing. One of these test is the >24 h polarization of the coated sheets at 0.6 V vs AgCl (0.823 V vs SHE). In this work it was decided to employ an 18 hour test routine. The tests were run in an aerated solution as recommended. For some of the tests, 18 hours were enough time to reach a steady-state current density. For the majority of the tests the current density was still declining after 18 hours, and longer durations would indisputably have yielded smaller current density values. The results obtained were however found illustrative enough to give a comparison of the behaviours of the coatings. The numerical values may be off, and if these are of importance, tests with a longer time frame is advised.

The linear sweep voltammetric measurements were run from -0.177 V to 0.823 V vs SHE. The pH of the solution was approximately 3 (1 mM H_2SO_4 solution). This means that at the lowest potentials, hydrogen gas may be formed. At pH 3 and $p_{H_2} = 1$ atm the hydrogen evolution can thermodynamically take place at -0.210 V vs SHE (see Appendix A.2). The real partial pressure of hydrogen is however much lower than 1 atm, and evolution of hydrogen gas is expected in the lower potential ranges. This also seems to be the case, since all the linear sweep curves obtained has a substantial current at the lowest potentials.

The electrolyte used in the electrochemical experiments is 1 mM H_2SO_4 at 80 $°C$. DOE in addition to this recommends an addition of 1 ppm HF to the solutions. It was chosen not to do this, as Sigrid Lædre in her master thesis showed that additions of F^--ions up to 2 ppm had no effect on the corrosion behaviour of 316L stainless steels [7]. This combined with the fact that HF is not a preferable chemical to use (highly corrosive and toxic), made us decide to omit it from the electrolyte. DOE recommends the electrolyte for the linear sweeps to be purged with an inert gas (argon). In this work we used nitrogen to remove any dissolved oxygen present in the electrolyte. For the potentiostatic measurements the electrolyte should be aerated, and no gas was therefore purged in the solution.

6.2 Effect of Addition of Zonyl to Coatings

6.2.1 Wetting Performance

The addition of Zonyl increased the contact angles measured between water droplets and the coatings for low concentrations (see Figure 5.35 and 5.36). The hydrophobicity decreased when the concentration becomes too high.

The increase was attributed to the fact that Zonyl is small particles of PTFE (PolyTetraFluorEthene), which is a very hydrophobic material. A larger concentration of hydrophobic material on the surface of the coating therefore made it repel water. This was true both for coatings containing graphite and carbon black, but also for the coatings with just epoxy (and Zonyl). The pure epoxy coating was more hydrophobic than the coatings with graphite/CB, and this is because the graphite and carbon black has a lower contact angle than pure epoxy. As the Cassie equation 3.13 predicts, the apparent contact angles therefore were lower for the coatings containing graphite/CB.

At higher concentrations of Zonyl (Figure 5.35 and 5.36), the hydrophobicity decreased again. The sizes of the Zonyl particles were larger than the other components in the mixture, and when they became too dominant, the roughening effect was lost. The average roughness fell from 3.16 μm to 2.99 μm as the Zonyl content increased from 4.8 vol% to 12.2 vol% (Figures 5.34 and 5.33).

When comparing Figure 5.32 to Figures 5.34 and 5.33, it can be seen that the addition of Zonyl to the coatings gave an increase in the average roughness. The roughness for the coating without Zonyl was found to be 1.48 μm, while the average roughness of the coatings with Zonyl was 3.16 and 2.99 μm. As given in section 3.6, a rougher surface also gives a more hydrophobic surface. This can partially explain the increase in contact angle for coatings with more Zonyl (Figures 5.35 and 5.36).

6.2.2 Bipolar Plate Ex-situ Testing

From Figure 5.24 there is not an apparent trend in the current densities as a function of Zonyl content. The results obtained can probably mostly be attributed to other factors than the Zonyl content in the coatings. A small decrease in current density can be seen for the coatings containing 12.2 vol% Zonyl, but the drop was too small to be said to be a definitive trend.

Figure 5.10 shows that small additions of Zonyl lowered the contact resistance of the coatings. This is interesting, since the Zonyl particles are electrically insulating. The theory is that the hydrophobicity of the particles make the coating solution more homogeneous, and spreads the graphite and carbon black particles more evenly. This prevents the particles from cluttering in the cured coating, and therefore increases the conductivity. As the concentration of Zonyl increases, the insulating nature of the particles

outweighs the positive mixing abilities and the contact resistance increases again. This is a well known consequence of reaching the percolation threshold [54].

Manually air brushing and mixing of the coatings does give rise to some randomness in the coatings, and this can also be cause for the decrease in contact resistance for the highest concentrations of Zonyl on the glass blasted plates in Figure 5.10.

6.3 Effect of Coating Thickness

From Table 5.1 we can see the resulting theoretical thicknesses of the coatings (calculated from the weight of the coatings). Hans Husby examined the cross sections of his coatings in his master thesis [6], and estimated a porosity of approximately 50 %. The coating used by Husby are similar to the ones used in this work, and a similar porosity is expected. That means the coatings can be up to double the theoretical thickness. The hot press pressure used in this work is however three times what was used in Hans Husby's work, and therefore a lower porosity is probable.

The thinnest coatings were found in series 7 and 8, and these coatings have either no particles added (pure epoxy) or the minimum amount of Zonyl added. This is a trivial fact, since addition of particles will indisputably increase the coating volume, and in turn the thickness of the of the coating.

The thickest coatings were series 9-12, which are the coatings that are put onto the glass blasted steel substrates. The improved adhesion between the plates and the coatings seems to have increased the amount of paint mixture that sticks to the plate. The air brush used to spray the paint onto the plates was changed before spraying series 9-12, but the new gun was the exact same type as the gun used to spray the other plates. It can however not be excluded that there might be some difference between the guns used, and that this has an effect on the thickness of the prepared coatings.

There is no apparent correlation between the coating thickness and the contact resistance measured, as seen from Figure 5.11. This was also a conclusion drawn by Hans Husby in his master thesis [6].

No trend is seen for the current densities obtained from the potentiodynamic measurements at -0.1 V vs SHE (Figure 5.22) either. This is however expected, since at these low absolute potentials the coating materials or

plate is not thermodynamically in danger of reacting.

From the linear sweep scans performed on the uncoated stainless steel (Figure 5.12), very little corrosion was recorded. The current density measured at the most negative potentials is evolution of hydrogen gas. The current densities measured below the open circuit potential is probably reduction of oxygen gas in the electrolyte or in pores of the coating.

From Figure 5.23 there seems to be a correlation between the current density and the coating thickness in the potentiostatic measurements taken at +0.823 V vs SHE. The current density increased with increasing coating thickness. This might indicate that carbon corrosion was happening in the coating, and that the thicker coatings had more available carbon for corrosion. There might also be other corrosion processes occurring, like crevice corrosion on the exposed steel underneath the coating.

The increased thickness of the coating makes crevices in the coating deeper. This separates the bottom of the crevice more from the rest of the electrolyte, and the concentrations of the dissolved metal ions increases. As shown in section 3.4.3, when the concentration of metal ions get high enough, the ions react with water creating hydroxides and protons (equations 3.9 and 3.10). This lowers the pH in the crevice, and accelerates corrosion. The build-up of the oxide layer contributes to increasing the contact resistance after the electrochemical measurements.

Hans Husby [6] also found a correlation between the coating thickness and the potentiostatic corrosion current densities in his master thesis [6], and attributed the increase in current density to carbon corrosion. The measurements done in his work had lower potential and shorter measurement durations, but they are else comparable to the results obtained in this work.

Corrosion testing on coated gold plates gave the same trend with larger current density for the thickest coating (Figure 5.18). Contact resistance measurements after the electrochemical testing also gave higher results (Figure 5.2). The results were however not as high as the ones obtained from the coated stainless steel plates (Figure 5.8). The corrosion measured from the gold plates should therefore exclusively be carbon corrosion

The increase in contact resistance from the coated stainless steel plates seems to be a combination of the two mechanisms. The contact resistance increases because there is a build up of oxide layer on the metal, and the conductivity of the coating decreases as the carbon corrodes. De-lamination of the coating is also a factor to be considered, as reduction of the numbers

of participating conduction connection points between the graphite/CB in the coating and the metal sheet will greatly increase the contact resistance.

6.4 Effect of Surface Morphology

The surface characteristics of the substrate is a very important parameter when it comes to contact resistance. As seen from the SEM images (Figure 5.27 and 5.28), the surfaces of the substrates used this autumn and in this work were very different. The much coarser surface on the plates used in our previous master thesis project work [11] provided a much better adhesion for the coatings than what was the case with the new substrates. The contact resistances acquired from measurements of the old coated plates (Figure 3.13) showed lower contact resistances than what was obtained for any of the coatings tested in this work. The lines for 2043 N cm^{-2} are the closest results to the lines in Figure 5.3 with 0 vol% Zonyl. The contact resistance before electrochemical measurements was much lower on the old coated plates than what was obtained in the measurements done in this work.

Even though the glass blasted plates had a rough enough surface to keep the coating adhered (Figure 5.29), it did not get the same conductivity through the coating. The deeper cracks seen in the surface of the old plates seemed to provide better contact points (larger contact area) between the metal and the graphite particles in the coating (Figure 5.28). Where the old plates achieved the goals set by DOE both before and after the electrochemical testing (Figure 3.13), the new plates had higher values before electrochemical testing (Figure 5.6) and much higher after testing (Figure 5.8)

A possible explanation of the mechanism can be illustrated as attaching clay onto a surface; Pressing the clay against a smooth surface will result in it peeling off again pretty soon. A rough surface will hold better, but still it will not sit indefinitely. If the clay is compressed against a surface which has lots of deep grooves, the clay will be pressed into the grooves and this anchors the clay in the surface.

The contact points inside the grooves also seem to persist after the electrochemical testing, perhaps because they are better shielded from the electrolyte. The glass blasted plates does not have this shielding of contact points, and even though the coating does not peel off, the contact between

the metal and graphite particles seems to worsen and the contact resistance increases. Figure 6.1 gives a sketch of the two situations.

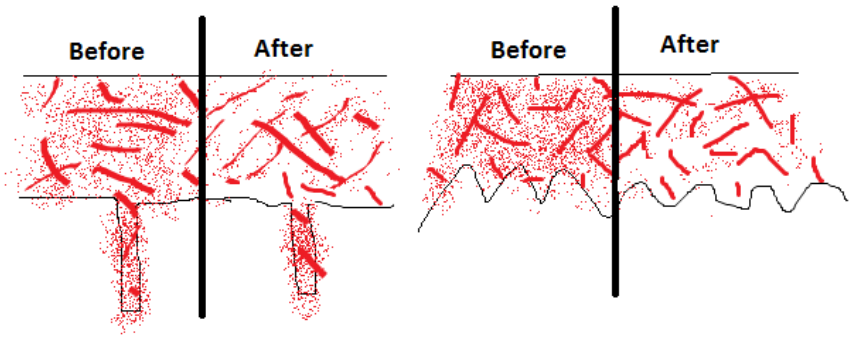

Figure 6.1: The image to the left is the situation with the old plates before and after the electrochemical testing. The image to the right gives the situation with the glass blasted substrates before and after electrochemical testing. The large red "fibres" are the graphite particles and the small red dots are the CB. The graphite and CB are shielded in the deep grooves on the surface, and even though electrolyte gets through the coating down to the surface, it does not advance into the grooves. This keeps a low contact resistance by retaining the steel/graphite bonds.

The effect described in Figure 6.1 can be used to explain both the low contact resistance before electrochemical testing (the increased contact area), and the retaining of this low contact resistance after electrochemical measurements (electrolyte does not get into the grooves). This can also explain why the contact resistances measured by Hans Husby [6] were so high before the coatings were compressed, but suddenly became very good as the coating was compressed before curing. The coatings compressed after curing had an improvement, but not as radically as the un-cured coatings. This is because the cured coatings did not get pushed into the grooves during pressing, but the un-cured coating did.

It seems mechanical adhesion of the coating is extremely important in order to achieve good contact resistance. Coating pressed into the grooves of the metal substrate anchors the coating to the substrate, as well as shield it. If electrolyte penetrates the coating, the coating pressed into the grooves will be protected, and therefore maintain good contact resistance even after the electrochemical testing.

6.5 General

It is difficult to make a coating that performs well both before and after the electrochemical testing. None of the coatings developed during this work performed good enough ex-situ to achieve the goals set by DOE [15].

The increase in contact resistance after the electrochemical measurements is believed to be caused partly by formation of an oxide layer on the metal underneath the coating, and partly by the fact that carbon corrosion removes the conductive paths through the coating. The gold plate with the thickest coating had a significant increase in contact resistance after the electrochemical testing (Figure 5.2), and since gold does not produce an oxide layer at these conditions, the increase can not come from this. The increased contact resistance must therefore come from deterioration of the coating itself.

During the electrochemical measurements carbon corrosion removes some of the CB in the coating. Even though the graphite is responsible for most of the conductivity in the coating, the CB functions as connection points between the graphite particles. When these points disappear, a lower electrical conductivity through the coating is the result.

When comparing the glass blasted sheets (Figure 5.8) with the bipolar plates

used in the project work (Figure 3.13), the glass blasted plates have a larger increase in contact resistance after electrochemical measurements. This is because these have no "shielded" contact points beneath the surface. The glass blasted plates were also held at a high potential (0.823 V vs SHE) for 18 hours, and thus experienced a lot more carbon corrosion than the old plates that were swept from -0.34 V to 0.76 V vs SHE at a rate of 2 mV s^{-1}.

Cracks in the coating and porosity enables the electrolyte to come in contact with the metal substrate underneath the coating. These areas will then be oxidized. For stainless steels this layer will consist mostly of insulating chromium oxide. This will make the contact resistance increase and reduce the current efficiency. The area oxidized should however be limited, as most of the substrate is covered by the coating. The increase in contact resistance should therefore not be too high.

If the cracks in the coating are thin enough and deep enough they can initiate crevice corrosion. Crevice corrosion greatly accelerates the corrosion and oxide formation by altering the acidity in the crack. As seen from equations (3.9) and (3.10), when the metal ion concentrations get high enough, the environment gets more acidic. Since the crevices promote galvanic corrosion, metal ions will be let into the solution inside the crevice, while the reduction happens somewhere else. A thicker coating will have deeper cracks and therefore more corrosive conditions in the cracks. This can explain Figure 5.23 which show the increase in corrosion currents measured with the increase in coating thickness.

Another mechanism that increases the contact resistance is carbon corrosion. The crystalline graphite particles are the predominant charge conductors in the composite, but the particles are large and interconnected by the smaller and more amorphous carbon black particles. These have a higher tendency of corrosion, and even though they do not conduct a large portion of the current, loss of the interconnects between the graphite particles decrease the conductivity through the coating, and thus increases the contact resistance.

At its most extreme, carbon corrosion might remove practically all connection points between the graphite particles. This would give a prominent increase in contact resistance. Figure 5.9 gives the contact resistances of the 304 stainless steel plates after electrochemical measurements. The coating with 12.2 vol% Zonyl has a very high contact resistance until it reaches $\sim$ 300 N cm^{-2}. Then the contact resistance suddenly drops to very low val-

ues. This drop was also seen when repeating the measurement. The reason for this change may be that carbon corrosion has removed practically all the CB particles connecting two layers of graphite. The contact resistance is then very high. As the compression pressure increases, the conducting layers are pressed together. At some point the two layers of graphite are forced in contact with one another, and the contact resistance experience a steep drop as the conductivity suddenly increases.

From the SEM images of the coated glass blasted sheets (Figures 5.30 and 5.31), it seems the upper layer (probably predominantly epoxy) is removed during electrochemical measurements. More CB particles are seen in the image after electrochemical measurements, and this might indicate a more "transparent" surface for the electrons in SEM (not blocked by insulating epoxy). This in itself should lower the contact resistance, but for the reasons discussed above, no such improvement is measured.

Chapter 7

Conclusion

A carbon based coating consisting of graphite and CB dispersed in an epoxy-polymer with the addition of PTFE-particles was developed in order to meet the requirements set by DOE for 2020. The coatings were applied to 316L stainless steel and 304 stainless steel metal sheets by airbrushing, and cured in a hot press at 110 $°C$ for 30 min at 2670 N cm^{-2} in order to remove as much porosity as possible.

Addition of Zonyl did not prevent the electrolyte from direct contact with the metal plates from forming an oxide layer. The increase in contact resistance after polarizing the plates at 0.823 V vs SHE for 18 hours was very high, with results ranging from 50 mΩ cm^2 to over 300 mΩ cm^2 at a compaction pressure of 147 N cm^{-2}. This was high above the goals from DOE, which is a contact resistance of less than 10 mΩ cm^2 at 138 N cm^{-2} (200 psi).

The degradation mechanism for the coated sheets was determined to be a combination of carbon corrosion and oxide formation on the metal surface, as well as de-lamination of the coating. Both carbon corrosion and oxide formation are dependent on the thickness of the coating. A thick coating has more available carbon for corrosion, and also facilitates deeper crevices in which crevice corrosion can occur, but prevents the electrolyte from direct contact with the metal.

Pretreatment of the sheets before coating is important in order to achieve good adhesion between the plate and the coating. Glass blasting with particles with a particle size of about 50 μm provided a rougher surface for the coating, and it stuck a lot better than what was the case for the as-prepared

plates.

The contact resistance was not retained after electrochemical measurements, as was achieved (at least for most of the coatings) in the project work. The reason for this was argued to be the difference in surface morphology of the plates used in this work and in the project work. The project work plates had a surface in which the coating could be pressed into voids, and by that ”anchor” itself in the coating. This effect provided good adhesion of the coating, as well as shielding the coating pressed into the plate. The coating in the anchor points therefore seemed to retain conduction between the plate and the coating, even after electrochemical measurements. This effect is encouraged for further studies, as no available (as per June 2013) work can be found on the subject.

Chapter 8

Further Work

Addition of PTFE to the coatings did not prove particularly successful to improve the corrosion resistance. Addition of the PTFE after the carbon/epoxy mixture has been applied might prove more hydrophobic than mixing the PTFE-particles into the mixture.

The corrosion resistance could also be improved by removing any excess porosity in the coating. If the water/solution does not come in contact with the steel bipolar plate, it will not corrode. There might be many courses towards minimizing porosity. The epoxy/carbon mixing ratio can be optimized further (although this has previously been investigated to some extent by Hans Husby [6]). A combination of largeer and smaller graphite particles might also provide closer packing and thus lower porosity. High pressures during curing of the coating proved successful (as shown in the project work of the author [11]), and even higher pressures might further improve the removal of porosity.

Compressing the GDL into the coating before it has cured has been proved by the research group to give promising results. Hans Husby has described the concept in his master thesis [6], and a patent is currently being filed by SINTEF and its partners. If the concept still proves promising, work should be put into developing it further to see how good the bipolar plates can become.

The ex-situ results obtained can also be misleading, and testing of the coatings in-situ is highly recommended. It is difficult to create good ex-situ tests that can mimic the environment experienced by the bipolar plates inside the PEM fuel cell. Work should be put into devising good tests that correlate

well to the results obtained in actual operation.

The surface roughness and morphology has in this work been identified as one of the key parameters when it comes to achieving a low contact resistance. The plates prepared in the project work during the fall of 2012 performed better than the new plates before electrochemical measurements and much better after electrochemical measurements. The reason is believed to be the deeper valleys found in the old bipolar plates (Figure 5.28 vs 5.27). A study to determine the effects of the morphology and roughness should be conducted to clarify its importance. Plates could be made with grooves of different depths and sizes by controlled chemical etching or another suitable method before coating and compressing.

It is common to pretreat bipolar plates before coating by sand blasting or by chemical methods, but no articles were found (as per June 2013) on controlled morphology effects on coating performance.

Bibliography

[1] C. C. Chan, "The state of the art of electric, hybrid, and fuel cell vehicles," *Proceedings of the IEEE*, vol. 95, no. 4, pp. 704–718, 2007.

[2] T. Fukutsuka, T. Yamaguchi, Y. Matsuo, Y. Sugie, and Z. Ogumi, "Improvement in corrosion properties of carbon-coated fe-based metals for pefc bipolar plate," *Electrochemistry (Tokyo, Jpn.)*, vol. 75, no. 2, pp. 152–154, 2007.

[3] S. Joseph, J. C. McClure, R. Chianelli, P. Pich, and P. J. Sebastian, "Conducting polymer-coated stainless steel bipolar plates for proton exchange membrane fuel cells (pemfc)," *International Journal of Hydrogen Energy*, vol. 30, no. 12, pp. 1339–1344, 2005.

[4] A. P. Nowak, T. T. Salguero, K. W. Kirby, F. Zhong, and R. H. J. Blunk, "A conductive and hydrophilic bipolar plate coating for enhanced proton exchange membrane fuel cell performance and water management," *Journal of Power Sources*, vol. 210, no. 0, pp. 138–145, 2012.

[5] S. Kitta, H. Uchida, and M. Watanabe, "Metal separators coated with carbon/resin composite layers for pefcs," *Electrochimica Acta*, vol. 53, no. 4, pp. 2025–2033, 2007.

[6] H. Husby, "Carbon coatings for bipolar plates in pem fuel cells, msc thesis," 2012.

[7] S. Laedre, "Investigation of metal bipolar plates for use in pem fuel cells, msc thesis," 2011.

[8] J. Larminie and A. Dicks, *Fuel cell systems explained*. Chichester: Wiley, 2003.

[9] A. Kirubakaran, S. Jain, and R. K. Nema, "A review on fuel cell technologies and power electronic interface," *Renewable Sustainable Energy Rev.*, vol. 13, no. 9, pp. 2430–2440, 2009. CAN 153:435683 Electrochemical, Radiational, and Thermal Energy Technology.

[10] H. Tawfik, Y. Hung, and D. Mahajan, "Metal bipolar plates for pem fuel cell-a review," *Journal of Power Sources*, vol. 163, no. 2, pp. 755–767, 2007.

[11] H. Husby, "Carbon composite coating for bipolar plates in pem fuel cells, msc thesis project work." December 2012.

[12] L. Carrette, K. A. Friedrich, and U. Stimming, "Fuel cells: Principles, types, fuels, and applications," *ChemPhysChem*, vol. 1, no. 4, pp. 162–193, 2000.

[13] S. Bourne, "Itm's membrane technology unlocks the power of hydrogen," *Fuel Cells Bulletin*, vol. 2012, no. 7, pp. 12 – 15, 2012.

[14] H. Tsuchiya and O. Kobayashi, "Mass production cost of pem fuel cell by learning curve," *International Journal of Hydrogen Energy*, vol. 29, no. 10, pp. 985–990, 2004.

[15] D. of Energy, "Hydrogen, fuel cells & infrastructure technologies programme," 2011.

[16] J. Healy, C. Hayden, T. Xie, K. Olson, R. Waldo, M. Brundage, H. Gasteiger, and J. Abbott, "Aspects of the chemical degradation of pfsa ionomers used in pem fuel cells," *Fuel Cells*, vol. 5, no. 2, pp. 302–308, 2005.

[17] A. Hermann, T. Chaudhuri, and P. Spagnol, "Bipolar plates for pem fuel cells: A review," *International Journal of Hydrogen Energy*, vol. 30, no. 12, pp. 1297–1302, 2005.

[18] J. Wind, R. Späh, W. Kaiser, and G. Böhm, "Metallic bipolar plates for pem fuel cells," *Journal of Power Sources*, vol. 105, no. 2, pp. 256 – 260, 2002. 7th Ulmer Elektrochemische Tage.

[19] H. Wang, M. A. Sweikart, and J. A. Turner, "Stainless steel as bipolar plate material for polymer electrolyte membrane fuel cells," *Journal of Power Sources*, vol. 115, no. 2, pp. 243–251, 2003.

[20] P. D. Harvey, *Engineering properties of steel.* American Society for Metals Metals Park, Ohio, 1982.

[21] C. Spiegel, "Designing and building fuel cells," 2007.

[22] C.-C. Shih, C.-M. Shih, Y.-Y. Su, L. H. J. Su, M.-S. Chang, and S.-J. Lin, "Effect of surface oxide properties on corrosion resistance of 316l stainless steel for biomedical applications," *Corrosion Science*, vol. 46, no. 2, pp. 427 – 441, 2004.

[23] A. E. Yaniv, J. B. Lumsden, and R. W. Staehle, "The composition of passive films on ferritic stainless steels," *Journal of The Electrochemical Society*, vol. 124, no. 4, pp. 490–496, 1977.

[24] H.-S. Oh, K. H. Lim, B. Roh, I. Hwang, and H. Kim, "Corrosion resistance and sintering effect of carbon supports in polymer electrolyte membrane fuel cells," *Electrochimica Acta*, vol. 54, no. 26, pp. 6515–6521, 2009.

[25] J. Bockris, D. Drazic, and A. Despic, "The electrode kinetics of the deposition and dissolution of iron," *Electrochimica Acta*, vol. 4, pp. 325–361, Aug. 1961.

[26] R. Tunold, "Korrosjonslaere: forelesningsreferat," 1988.

[27] J. Hjelen, *Scanning elektron-mikroskopi*. Trondheim: SINTEF, 1989.

[28] H.-J. Butt, K. Graf, and M. Kappl, *Physics and chemistry of interfaces*. Weinheim: Wiley-VCH, 2006. 2nd, rev. and enlarged ed.

[29] J. Heikenfeld, "Electrowetting optics on target for record optical performance," *SPIE Newsroom*, 2008.

[30] A. M. Emel'yanenko and L. B. Boinovich, "Analysis of wetting as an efficient method for studying the characteristics of coatings and surfaces and the processes that occur on them: A review," *Inorg. Mater.*, vol. 47, no. 15, pp. 1667–1675, 2011.

[31] Y. Fu, M. Hou, H. Xu, Z. Hou, P. Ming, Z. Shao, and B. Yi, "Ag-polytetrafluoroethylene composite coating on stainless steel as bipolar plate of proton exchange membrane fuel cell," *Journal of Power Sources*, vol. 182, no. 2, pp. 580–584, 2008.

[32] R. H. Blunk, R. R. Quiel, A. P. Nowak, and D. W. Gorkiewicz, "Stable ultralyophobic coating for pemfc bipolar plate water management," November 2012.

[33] Y.-B. Lee, C.-H. Lee, and D.-S. Lim, "The electrical and corrosion properties of carbon nanotube coated 304 stainless steel/polymer composite

as pem fuel cell bipolar plates," *International Journal of Hydrogen Energy*, vol. 34, pp. 9781–9787, Dec. 2009.

[34] Y.-B. Lee and D.-S. Lim, "Electrical and corrosion properties of stainless steel bipolar plates coated with a conduction polymer composite," *Current Applied Physics*, vol. 10, pp. S18–S21, Mar. 2010.

[35] Y. Show, "Electrically conductive amorphous carbon coating on metal bipolar plates for pefc," *Surface and Coatings Technology*, vol. 202, pp. 1252–1255, Dec. 2007.

[36] Y. Show and K. Takahashi, "Stainless steel bipolar plate coated with carbon nanotube (cnt)/polytetrafluoroethylene (ptfe) composite film for proton exchange membrane fuel cell (pemfc)," *Journal of Power Sources*, vol. 190, pp. 322–325, May 2009.

[37] Y. Fu, G. Lin, M. Hou, B. Wu, Z. Shao, and B. Yi, "Carbon-based films coated 316l stainless steel as bipolar plate for proton exchange membrane fuel cells," *International Journal of Hydrogen Energy*, vol. 34, pp. 405–409, Jan. 2009.

[38] P. Yi, L. Peng, L. Feng, P. Gan, and X. Lai, "Performance of a proton exchange membrane fuel cell stack using conductive amorphous carbon-coated 304 stainless steel bipolar plates," *Journal of Power Sources*, vol. 195, pp. 7061–7066, Oct. 2010.

[39] C.-Y. Chung, S.-K. Chen, P.-J. Chiu, M.-H. Chang, T.-T. Hung, and T.-H. Ko, "Carbon film-coated 304 stainless steel as pemfc bipolar plate," *Journal of Power Sources*, vol. 176, pp. 276–281, Jan. 2008.

[40] W. L. Wang, S. M. He, and C. H. Lan, "Protective graphite coating on metallic bipolar plates for pemfc applications," *Electrochimica Acta*, vol. 62, pp. 30–35, 2012.

[41] J. R. Mawdsley, J. D. Carter, X. Wang, S. Niyogi, C. Q. Fan, R. Koc, and G. Osterhout, "Composite-coated aluminum bipolar plates for pem fuel cells," *Journal of Power Sources*, vol. 231, no. 0, pp. 106–112, 2013.

[42] M. S. Ismail, D. B. Ingham, L. Ma, and M. Pourkashanian, "The contact resistance between gas diffusion layers and bipolar plates as they are assembled in proton exchange membrane fuel cells," *Renewable Energy*, vol. 52, pp. 40–45, 2013.

[43] C. Turan, . N. Cora, and M. Koç, "Contact resistance characteristics of coated metallic bipolar plates for pem fuel cells - investigations on the

effect of manufacturing," *International Journal of Hydrogen Energy*, vol. 37, no. 23, pp. 18187–18204, 2012.

[44] R. C. Makkus, A. H. H. Janssen, B. F. A. de, and R. K. A. M. Mallant, "Use of stainless steel for cost competitive bipolar plates in the spfc," *J. Power Sources*, vol. 86, no. 1-2, pp. 274–282, 2000.

[45] A. Elhamid, M. H., Y. Mikhail, R. H. Blunk, and D. J. Lisi, "Corrosion resistant, electrically and thermally conductive coating for multiple applications," 2004.

[46] R. H. Blunk, K. W. Kirby, T. T. Salguero, and F. Zhong, "Conductive and hydrophilic coating for pemfc bipolar plate," November 2012.

[47] V. J. Guiheen, Z. Iqbal, D. Narasimhan, and T. Rehg, "Corrosion resistant coated fuel cell bipolar plate with graphite protective barrier and method of making the same," July 2003.

[48] Y. S. Jeong, Y. T. Jeon, J. H. Lee, and J. C. Park, "Metal separator plate for a fuel cell having a coating layer comprising carbon particles dispersed in a binder resin, and a production method therefore," 2009.

[49] R. G. Bates and V. E. Bower, "Standard potential of the silver-silver chloride electrode from 0 to 95 degrees c and the thermodynamic properties of dilute hydrochloric acid solutions.," *J. Res. Natl. Bur. Stand. (U. S.)*, vol. 53, pp. 283–90, 1954.

[50] W. J. Hamer and Y. C. Wu, "On the standard potential of the mercury: mercurous sulfate electrode at 25 degrees c in aqueous solution.," *J. Solution Chem.*, vol. 24, pp. 1013–24, 1995.

[51] S. Laedre, O. E. Kongstein, A. Oedegaard, F. Seland, and H. Karoliussen, "The effect of ph and halides on the corrosion process of stainless steel bipolar plates for proton exchange membrane fuel cells," *Int. J. Hydrogen Energy*, vol. 37, no. 23, pp. 18537–18546, 2012.

[52] K. Feng, Y. Shen, H. Sun, D. Liu, Q. An, X. Cai, and P. K. Chu, "Conductive amorphous carbon-coated 316l stainless steel as bipolar plates in polymer electrolyte membrane fuel cells.," *International Journal of Hydrogen Energy*, vol. 34, no. 16, pp. 6771–6777, 2009.

[53] K. Feng, X. Cai, H. Sun, Z. Li, and P. K. Chu, "Carbon coated stainless steel bipolar plates in polymer electrolyte membrane fuel cells.," *Diamond and Related Materials*, vol. 19, no. 11, pp. 1354–1361, 2010.

[54] M. Sumita, K. Sakata, S. Asai, K. Miyasaka, and H. Nakagawa, "Dispersion of fillers and the electrical conductivity of polymer blends filled with carbon black," *Polymer bulletin*, vol. 25, no. 2, pp. 265–271, 1991.

[55] R. E. Walpole, "Probability & statistics for engineers & scientists," 2012.

Appendix A

Appendices

A.1 Variance and Standard Deviation on Contact Angle Measurements

To get numeral values for the standard deviation and variance of the contact angle measurements are determined by using sample variance [55]. This is used when the full population of results are not known beforehand, and therefore needs to be determined. The variance of the population y (the results that could be obtained in the experiment) is defined as σ_y^2. See EQ A.1.

$$\sigma_y^2 = \frac{1}{n}\sum_{i=1}^{n}(y_i - \bar{y})^2 \tag{A.1}$$

Here, $\bar{y}$ denotes the average of the results obtained, EQ A.2

$$\bar{y} = \frac{1}{n}\sum_{i=1}^{n} y \tag{A.2}$$

The standard deviation is then the square root of σ (Eq A.1) as given in EQ A.3.

$$SD = \sigma = \sqrt{\sigma_y^2} \tag{A.3}$$

A.2 Thermodynamic Limit for Evolution of Hydrogen Gas

Hydrogen gas will in acidic environment evolve according to equation A.4

$$2H^+ + 2e^- \rightarrow H_2(g) \tag{A.4}$$

The standard reduction potential for this reaction is defined as 0 V vs SHE. To find the reversible potential for hydrogen evolution we use the Nernst equation A.5.

$$E^{rev} = E^0 - \frac{RT}{nF} \ln Q \tag{A.5}$$

Where E^{rev} is the reversible (half cell) potential, E^0 is the standard potential ($= 0V$), R is the gas constant, T is the absolute temperature (in Kelvin), n is the charges transferred in the reaction, F is Faradays number and Q is the reaction quotient. For this particular case $T = 353$ K, $n = 2$, $Q = \frac{a_{H_2}}{a_{H^+}}$. For calculations we approximate $a_{H^+} = c_{H^+}$, and $a_{H_2} = p_{H_2} = 1$. At pH = 3 the reversible potential thus become A.6.

$$E^{rev} = 0V - \frac{8.314\frac{J}{Kmol}353K}{2 \cdot 96485\frac{C}{mol}} \ln \frac{1}{\left(10^{-3}\right)^2} = -0.210V \tag{A.6}$$

Since the real partial pressure of hydrogen gas is much lower than 1 atm, the reversible potential is higher than what was calculated, and hydrogen will be evolved at the working electrode during operation in the lower potential range.

A.3 Compression Pressure in Hot Press

The press is set to 10 tons pressure. The area of the plates is 3.5X3.5 cm = 12.25 cm^2. There are three plates pressed at the same time. The compression experienced by the coatings can then be calculated as A.7:

$$P_C = \frac{10000kg}{3.5 \cdot 3.5cm^2 \cdot 3} 9.81\frac{N}{kg} = 2670\frac{N}{cm^2} \tag{A.7}$$

A.4 Contact Resistance Results

This section covers the comprehensive results obtained during the contact resistance measurements taken during this work.

Set up

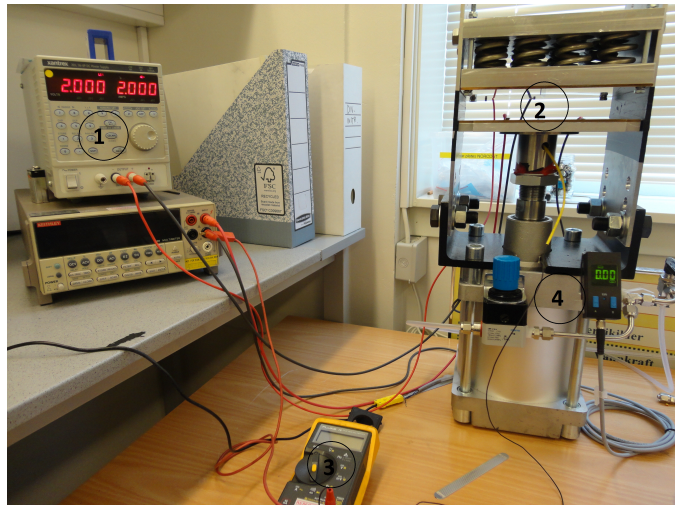

Figure A.1: Contact resistance set up used in this work. 1. Xantrax XDL 56-4P DC Power Supply" which force a current through the GDL and bipolar plate, 2. Input for the sample and GDL, 3. Mulitmeter to measure the voltage drop from the top plate to the pin, 4. Knob to adjust compaction pressure and display (measured in bar)

Before Electrochemical Testing

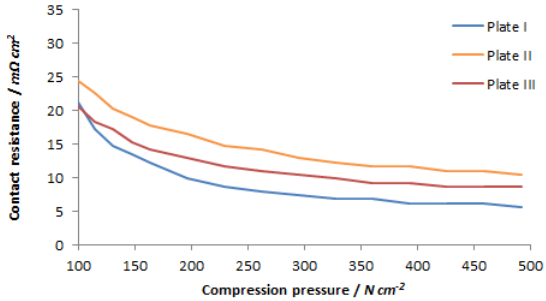

Figure A.2: Contact resistance measurements prior to electrochemical measurements on 316L stainless steel plates with 40 vol% graphite, 5 vol% carbon black and 55 vol% epoxy (0 % PTFE) coating

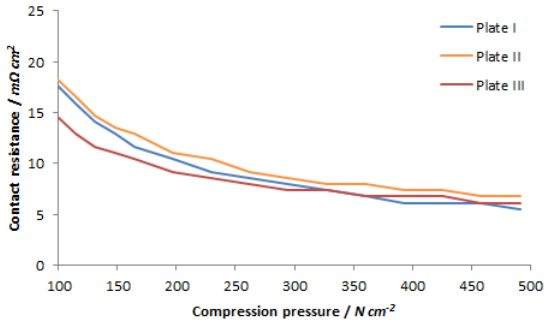

Figure A.3: Contact resistance measurements prior to electrochemical measurements on 316L stainless steel plates with 38 vol% graphite, 4.3 vol% carbon black, 4.8 vol% Zonyl and 53 vol% epoxy coating

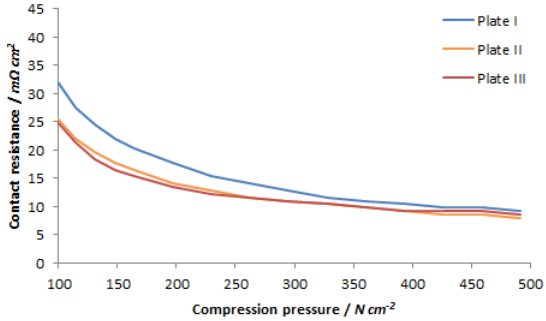

Figure A.4: Contact resistance measurements prior to electrochemical measurements on 316L stainless steel plates with 34.5 vol% graphite, 3.9 vol% carbon black, 13.2 vol% Zonyl and 48.4 vol% epoxy coating

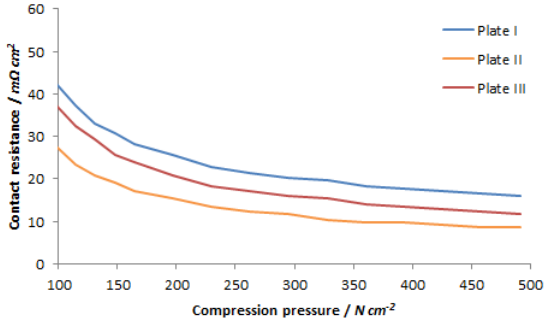

Figure A.5: Contact resistance measurements prior to electrochemical measurements on 316L stainless steel plates with 31.7 vol% graphite, 3.6 vol% carbon black, 20.2 vol% Zonyl and 44.5 vol% epoxy coating

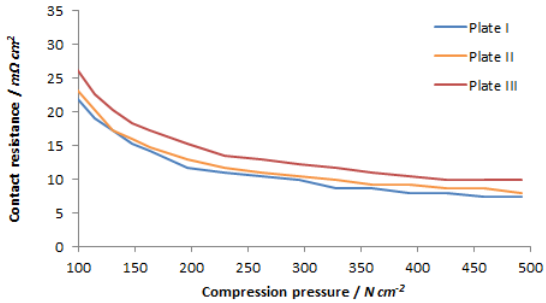

Figure A.6: Contact resistance measurements prior to electrochemical measurements on glass blasted 316L stainless steel plates with 40 vol% graphite, 5 vol% carbon black and 55 vol% epoxy (0 % PTFE) coating. Plate III is 304 grade steel

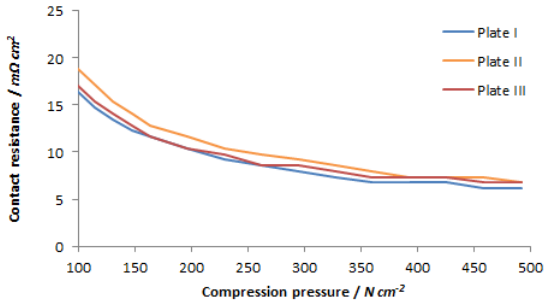

Figure A.7: Contact resistance measurements prior to electrochemical measurements on glass blasted 316L stainless steel plates with 38 vol% graphite, 4.3 vol% carbon black, 4.8 vol% Zonyl and 53 vol% epoxy coating. Plate III is 304 grade steel

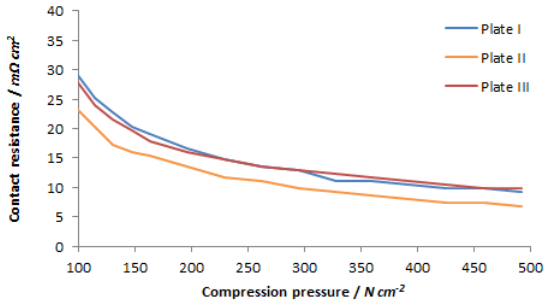

Figure A.8: Contact resistance measurements prior to electrochemical measurements on glass blasted 316L stainless steel plates with 34.5 vol% graphite, 3.9 vol% carbon black, 13.2 vol% Zonyl and 48.4 vol% epoxy coating. Plate III is 304 grade steel

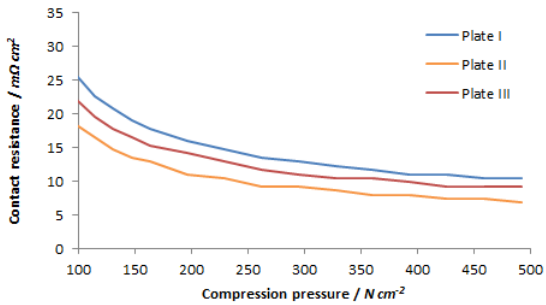

Figure A.9: Contact resistance measurements prior to electrochemical measurements on glass blasted 316L stainless steel plates with 31.7 vol% graphite, 3.6 vol% carbon black, 20.2 vol% Zonyl and 44.5 vol% epoxy coating

After Electrochemical Measurements

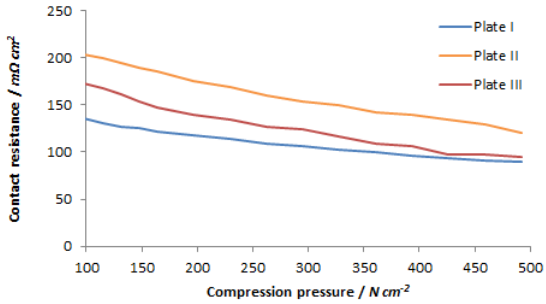

Figure A.10: Contact resistance measurements after electrochemical measurements on glass blasted 316L stainless steel plates with 40 vol% graphite, 5 vol% carbon black and 55 vol% epoxy (0 % PTFE) coating. Plate III is 304 grade steel

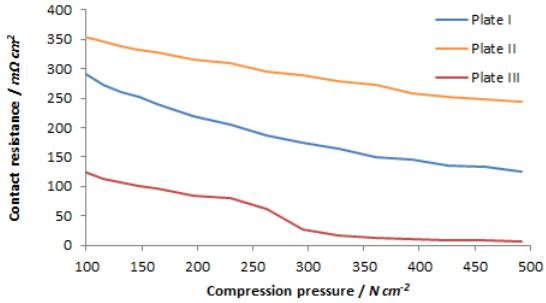

Figure A.11: Contact resistance measurements after electrochemical measurements on glass blasted 316L stainless steel plates with 38 vol% graphite, 4.3 vol% carbon black, 4.8 vol% Zonyl and 53 vol% epoxy coating. Plate III is 304 grade steel

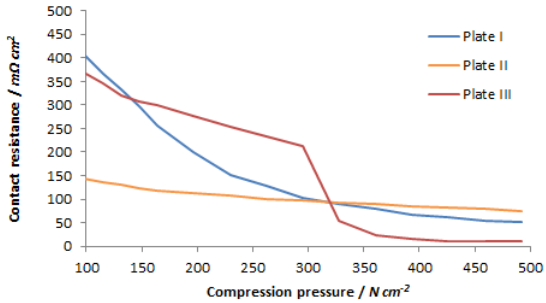

Figure A.12: Contact resistance measurements after electrochemical measurements on glass blasted 316L stainless steel plates with 34.5 vol% graphite, 3.9 vol% carbon black, 13.2 vol% Zonyl and 48.4 vol% epoxy coating. Plate III is 304 grade steel

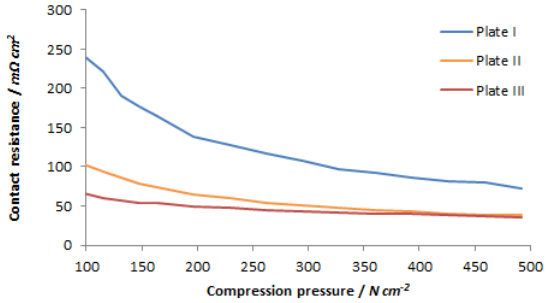

Figure A.13: Contact resistance measurements after electrochemical measurements on glass blasted 316L stainless steel plates with 31.7 vol% graphite, 3.6 vol% carbon black, 20.2 vol% Zonyl and 44.5 vol% epoxy coating

A.5 Linear Sweep

As-Delivered Steel Sheets

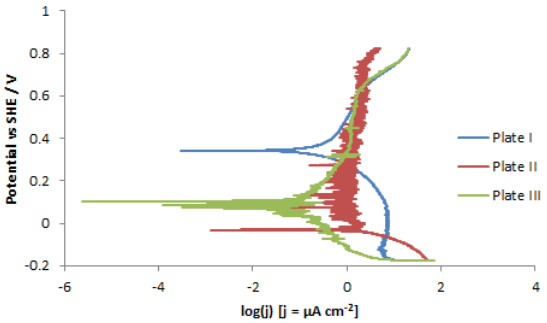

Figure A.14: Linear sweep voltammogram of 316L stainless steel plates coated with 40 vol% graphite, 5 vol% carbon black and 55 vol% epoxy (0 % PTFE). The sweep rate used was 0.1 mV s^{-1}, and the electrolyte was 1 mM H_2SO_4 at 80 $°C$.

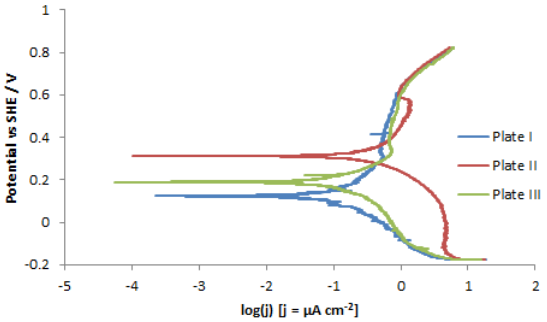

Figure A.15: Linear sweep voltammogram of 316L stainless steel plates coated with 38 vol% graphite, 4.3 vol% carbon black, 4.8 vol% Zonyl and 53 vol% epoxy. The sweep rate used was 0.1 mV s^{-1}, and the electrolyte was 1 mM H_2SO_4 at 80 $°C$.

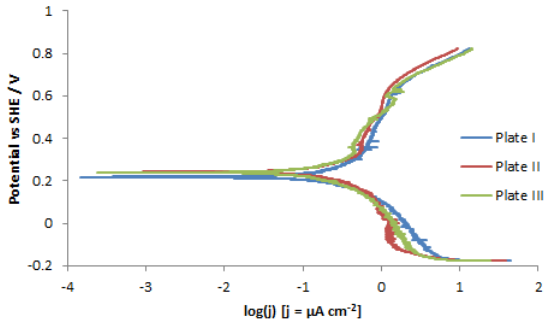

Figure A.16: Linear sweep voltammogram of 316L stainless steel plates coated with 34.5 vol% graphite, 3.9 vol% carbon black, 13.2 vol% Zonyl and 48.4 vol% epoxy. The sweep rate used was 0.1 mV s^{-1}, and the electrolyte was 1 mM H_2SO_4 at 80 $°C$.

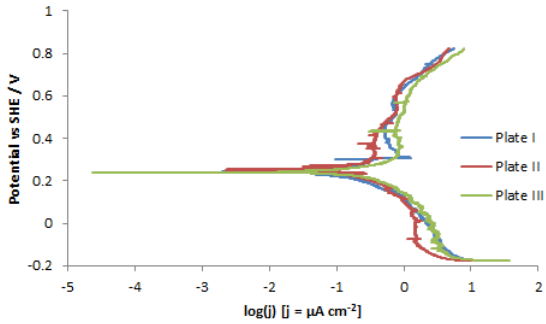

Figure A.17: Linear sweep voltammogram of 316L stainless steel plates coated with 31.7 vol% graphite, 3.6 vol% carbon black, 20.2 vol% Zonyl and 44.5 vol% epoxy coating. The sweep rate used was 0.1 mV s^{-1}, and the electrolyte was 1 mM H_2SO_4 at 80 $°C$.

Glass Blasted Steel Sheets

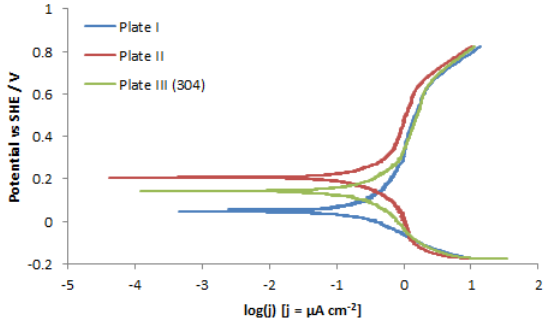

Figure A.18: Linear sweep voltammogram of glass blasted 316L stainless steel plates with 40 vol% graphite, 5 vol% carbon black and 55 vol% epoxy (0 % PTFE) coating. The sweep rate used was 0.1 mV s^{-1}, and the electrolyte was 1 mM H_2SO_4 at 80 $°C$. Plate III is 304 grade steel.

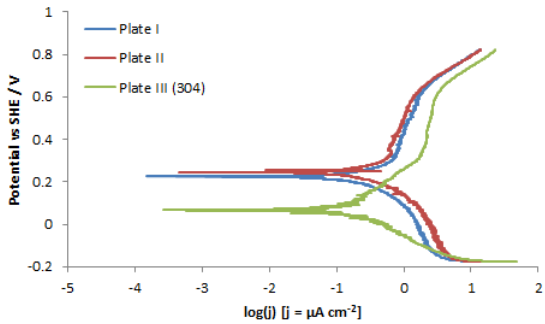

Figure A.19: Linear sweep voltammogram of glass blasted 316L stainless steel plates with 38 vol % graphite, 4.3 vol% carbon black, 4.8 vol% Zonyl and 53 vol% epoxy coating. The sweep rate used was 0.1 mV s^{-1}, and the electrolyte was 1 mM H_2SO_4 at 80 $°C$. Plate III is 304 grade steel.

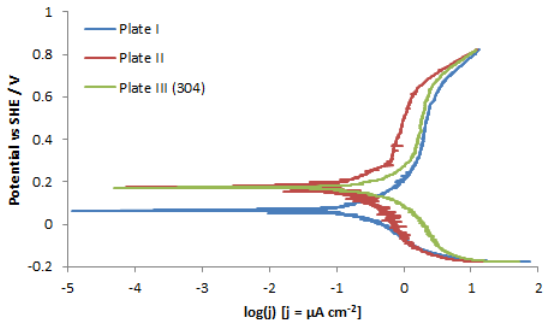

Figure A.20: Linear sweep voltammogram of glass blasted 316L stainless steel plates with 34.5 vol% graphite, 3.9 vol% carbon black, 13.2 vol% Zonyl and 48.4 vol% epoxy coating. The sweep rate used was 0.1 mV s^{-1}, and the electrolyte was 1 mM H_2SO_4 at 80 $°C$. Plate III is 304 grade steel.

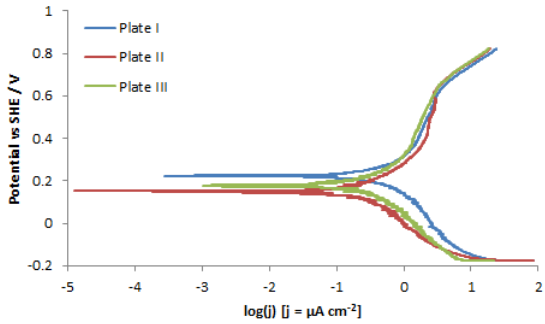

Figure A.21: Linear sweep voltammogram of glass blasted 316L stainless steel plates with 31.7 vol% graphite, 3.6 vol% carbon black, 20.2 vol% Zonyl and 44.5 vol% epoxy coating. The sweep rate used was 0.1 mV s^{-1}, and the electrolyte was 1 mM H_2SO_4 at 80 $°C$.

A.6 Chronoampereometry

As-Delivered Steel Sheets

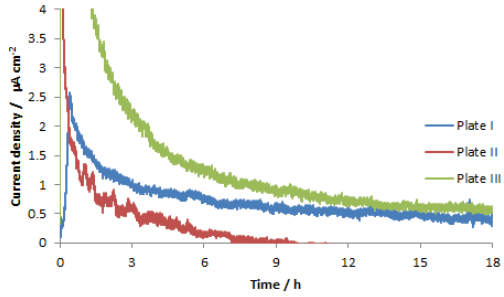

Figure A.22: Chronoampereometry of 316L stainless steel plates with 40 vol% graphite, 5 vol% carbon black and 55 vol% epoxy (0 % PTFE) coating. The test was taken for 18 hours at 0.823V vs SHE, and the electrolyte was 1 mM H_2SO_4 at 80 $°C$.

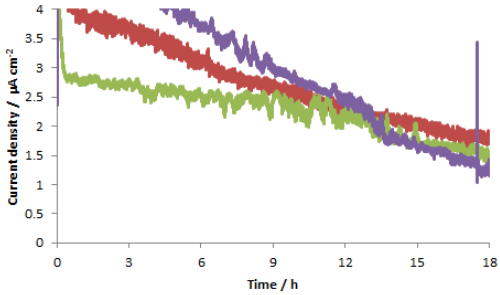

Figure A.23: Chronoampereometry of 316L stainless steel plates with 38 vol% graphite, 4.3 vol% carbon black, 4.8 vol% Zonyl and 53 vol% epoxy coating. The test was taken for 18 hours at 0.823V vs SHE, and the electrolyte was 1 mM H_2SO_4 at 80 $°C$.

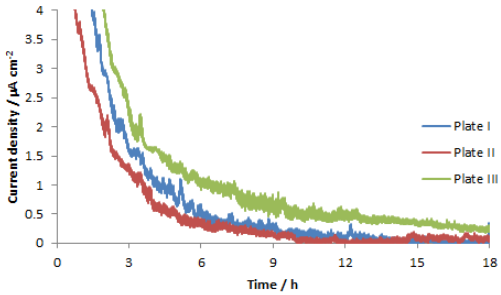

Figure A.24: Chronoampereometry of 316L stainless steel plates with 34.5 vol% graphite, 3.9 vol% carbon black, 13.2 vol% Zonyl and 48.4 vol% epoxy coating. The test was taken for 18 hours at 0.823V vs SHE, and the electrolyte was 1 mM H_2SO_4 at 80 $°C$.

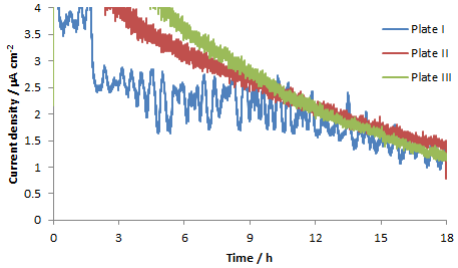

Figure A.25: Chronoampereometry of 316L stainless steel plates with 31.7 vol% graphite, 3.6 vol% carbon black, 20.2 vol% Zonyl and 44.5 vol% epoxy coating. The test was taken for 18 hours at 0.823V vs SHE, and the electrolyte was 1 mM H_2SO_4 at 80 $°C$.

Glass Blasted Steel Sheets

Mark: The y-axis has a different scale than the graphs in the previous subsection.

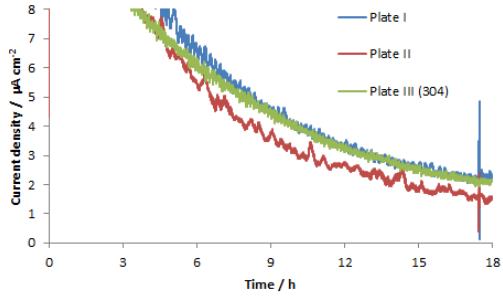

Figure A.26: Chronoampereometry of glass blasted 316L stainless steel plates with 40 vol% graphite, 5 vol% carbon black and 55 vol% epoxy (0 % PTFE) coating. The test was taken for 18 hours at 0.823V vs SHE, and the electrolyte was 1 mM H_2SO_4 at 80 $°C$. Plate III is 304 grade steel.

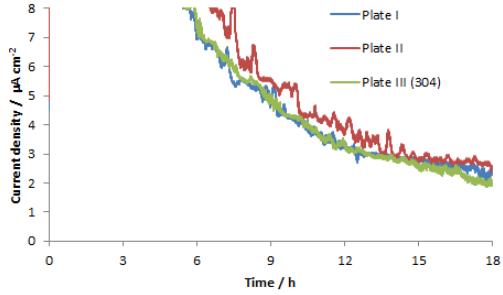

Figure A.27: Chronoampereometry of glass blasted 316L stainless steel plates with 38 vol% graphite, 4.3 vol% carbon black, 4.8 vol% Zonyl and 53 vol% epoxy coating. The test was taken for 18 hours at 0.823V vs SHE, and the electrolyte was 1 mM H_2SO_4 at 80 $°C$. Plate III is 304 grade steel.

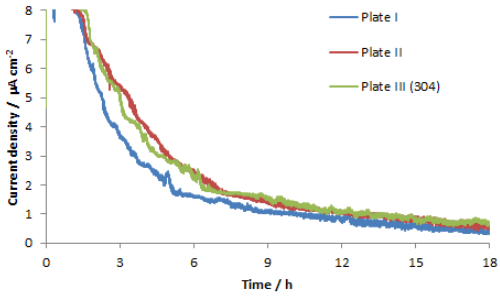

Figure A.28: Chronoampereometry of glass blasted 316L stainless steel plates with 34.5 vol% graphite, 3.9 vol% carbon black, 13.2 vol% Zonyl and 48.4 vol% epoxy coating. The test was taken for 18 hours at 0.823V vs SHE, and the electrolyte was 1 mM H_2SO_4 at 80 $°C$. Plate III is 304 grade steel.

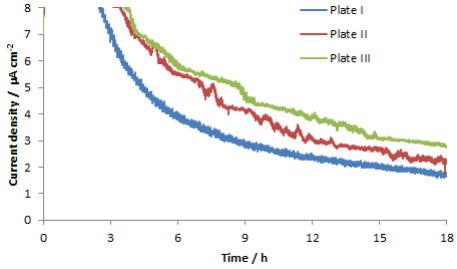

Figure A.29: Chronoampereometry of glass blasted 316L stainless steel plates with 31.7 vol% graphite, 3.6 vol% carbon black, 20.2 vol% Zonyl and 44.5 vol% epoxy coating. The test was taken for 18 hours at 0.823V vs SHE, and the electrolyte was 1 mM H_2SO_4 at 80 $°C$.

A.7 Scanning Electron Microscopy Images

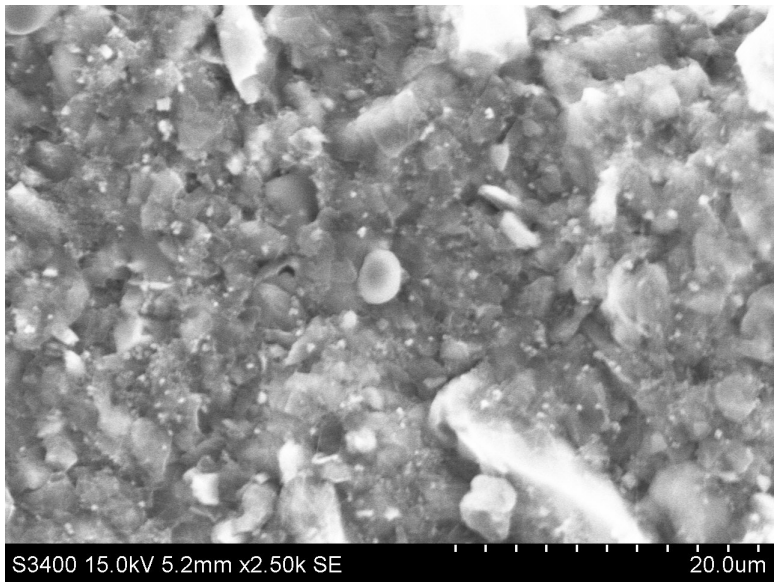

Figure A.30: Scanning electron microscopy image of coating with 34.5 vol% graphite, 3.9 vol% carbon black, 13.2 vol% Zonyl and 48.4 vol% epoxy

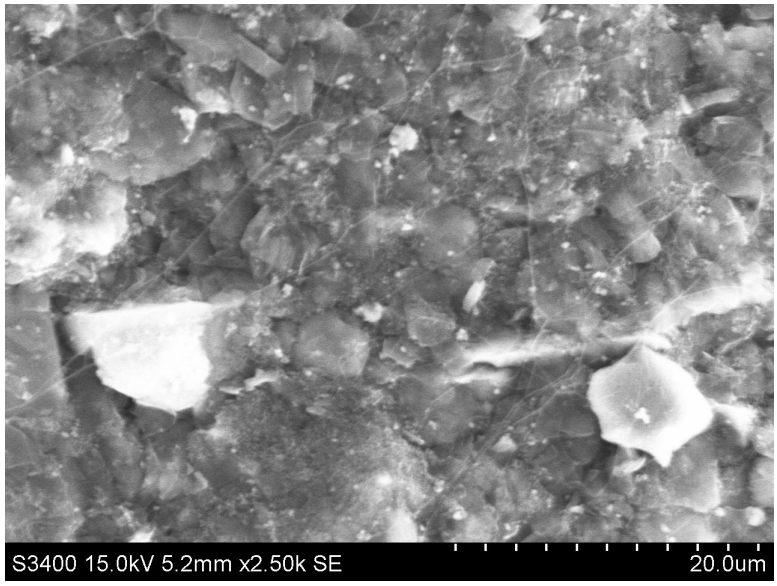

Figure A.31: Scanning electron microscopy image of coating with 38 vol% graphite, 4.3 vol% carbon black, 4.8 vol% Zonyl and 53 vol% epoxy

A.8 Plates As-delivered and Glass Blasted

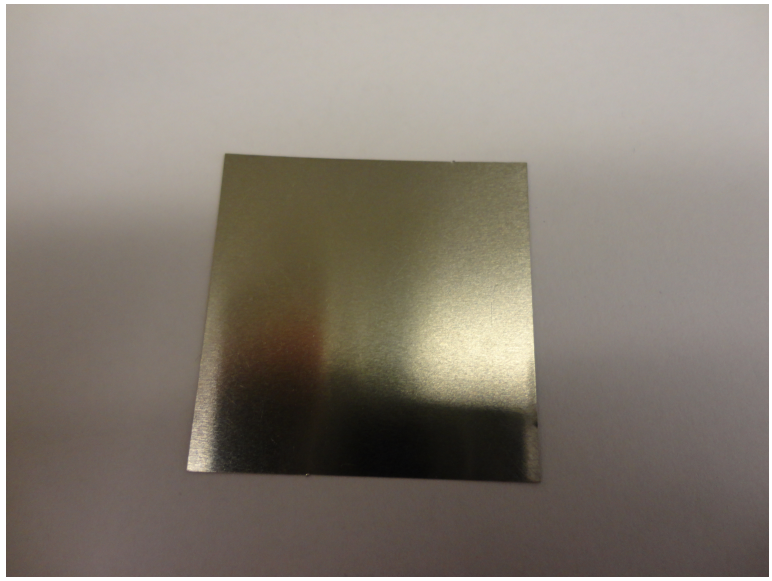

Figure A.32: Photography of 316L stainless steel plate supplied by ElringKlinger

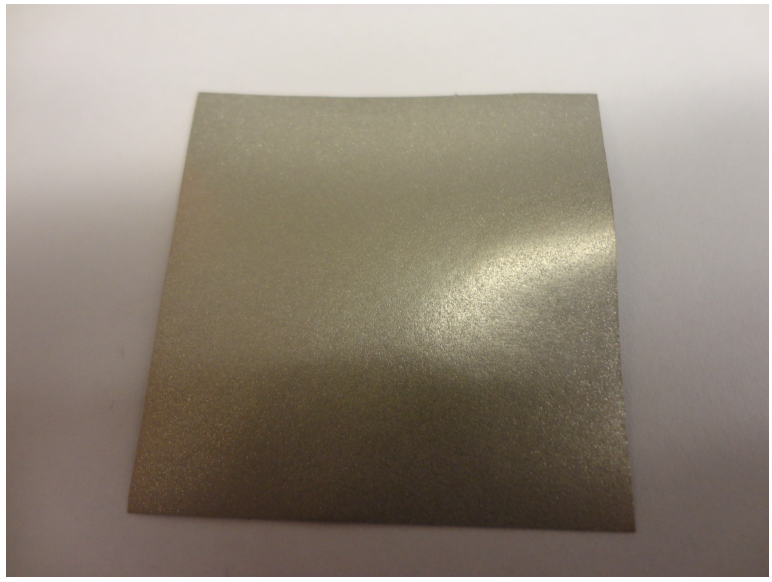

Figure A.33: Photography of glass blasted 316L stainless steel plate supplied by ElringKlinger